ELSEVIER

Chemical Geology 167 (2000) 193–229

CHEMICAL GEOLOGY
INCLUDING
ISOTOPE GEOSCIENCE

www.elsevier.com/locate/chemgeo

# Magnetite surface charge studies to 290°C from in situ pH titrations

David J. Wesolowski [a,*], Michael L. Machesky [b], Donald A. Palmer [a], Lawrence M. Anovitz [a]

[a] *Chemical and Analytical Sciences Division, Oak Ridge National Laboratory, P.O. Box 2008, Oak Ridge, TN 37831-6110, USA*
[b] *Illinois State Water Survey, 2204 Griffith Drive, Champaign, IL 61820, USA*

Received 7 July 1999

**Abstract**

The proton-induced surface charge of magnetite was investigated in 0.03 and 0.30 molal sodium trifluoromethanesulfonate solutions from 25°C to 290°C by potentiometric titrations using a stirred hydrogen electrode concentration cell. Pure magnetite with excellent crystallinity was produced by reaction with the $Ni/NiO/H_2O$ hydrogen fugacity buffer at 500°C. Inflection points in the 0.03 molal proton sorption isotherms ($pH_{infl}$) at 6.50, 6.24, 5.65, 5.47, 5.31 and 5.55 at temperatures of 50°C, 100°C, 150°C, 200°C, 250°C and 290°C, respectively, were used as estimates of the pristine point of zero charge ($pH_{ppzc}$) for modeling purposes. These $pH_{infl}$ values parallel $1/2\ pK_w$ and agree within the assigned uncertainty ($\pm 0.3$ pH units) at all temperatures with independent estimates of the $pH_{ppzc}$ calculated from an extension of 88the revised MUSIC model. The surface charging can be adequately described by a one-p$K$ model with a surface protonation constant fitted to the $pH_{infl}$ values, and giving the standard state thermodynamic properties $\log K_{H,298} = 7.00$, $\Delta H_{298}^{\circ} = -32.4 \pm 0.8$ kJ/mol and constant $\Delta C_p = 128 \pm 16$ J $K^{-1}$ $mol^{-1}$, with $\Delta S_{298}^{\circ}$ assumed to be equal to that of rutile protonation ($25.5 \pm 3.4$ J $K^{-1}$ $mol^{-1}$. The 0.03 and 0.30 molal proton sorption isotherms also exhibit pHs of common intersection ($pH_{cip}$) at 6.33, 5.78, 5.37, 4.82, 4.62 and 4.90 at 50°C, 100°C, 150°C, 200°C, 250°C and 290°C, respectively. The difference between the $pH_{cip}$ and $pH_{ppzc} \cong pH_{infl}$ values can be related to specific binding of $Na^+$ on the negatively charged surface, which increases with increasing temperature, although the $pH_{cip}$ values may also be affected by dissolution of the solid. The electrical double layer model includes a basic Stern layer capacitance, with specific cation and anion binding at the Stern layer, and a fixed diffuse layer capacitance computed from Guoy–Chapman theory. To fit the steepness and asymmetry of the charging curves above the $pH_{ppzc}$, an additional cation binding constant was invoked, which allows the cation to experience the surface potential. Significant kinetically controlled dissolution of magnetite was observed below the $pH_{ppzc}$, which may be a result of leaching of $Fe^{2+}$ from the surface, to produce a magnetite + hematite assemblage, despite the high hydrogen partial pressures (ca. 10 bars) used in these experiments. 

*Keywords:* Magnetite; Point of zero charge; Surface protonation; Potentiometric titration

* Corresponding author. Tel.: +1-865-574-6903; fax: +1-865-574-4961.
*E-mail address:* dqw@ornl.gov (D.J. Wesolowski).

0009-2541/00/$ - see front matter 
PII: S0009-2541(99)00209-0

## 1. Introduction

The adsorption of ions on solid surfaces is a fundamental phenomenon that influences many hydrothermal processes occurring in subsurface geological environments, including mineral dissolution and precipitation kinetics, the transport of colloidal particles, and the migration of cations and anions (organic and inorganic) through porous media. Magnetite, $Fe_3O_4$, is the stable oxide of iron in moderately to strongly reducing environments, including anoxic sedimentary formations, many hydrothermal and geothermal systems, primary exhalative and magmatic iron ores, and most igneous and metamorphic rocks. Although the surface charge and sorbtive characteristics of the fully oxidized Fe(III) iron oxides and hydroxides have been intensively studied at room temperature (cf. Parks, 1965; Dzombak and Morel, 1990), studies with magnetite have been considerably more limited (Parks, 1965; Tewari and McLean, 1972; Regazzoni et al., 1983; Blesa et al., 1984; Catalette et al., 1998; Mathur and Venkataramani, 1998; Marmier et al., 1999; Shen et al., 1999; and references to earlier work within these articles).

The application of potentiometric titration measurements for investigating the acid–base behavior of the solid/water interface may be traced to the Dutch school of colloid chemists in the 1950s (Mackor, 1951; Lyklema, 1961). Subsequently, deBruyn and his colleagues considerably refined the techniques (Parks and de Bruyn, 1962; Onoda and de Bruyn, 1966). Magnetite, hematite and, rutile are the only naturally occurring minerals for which the proton-induced surface charging properties have been investigated over an extended range of temperatures by direct pH titrations (Berube and de Bruyn, 1968; Tewari and McLean, 1972; Blesa et al., 1984; Fokkink et al., 1989). These and a few other oxides and hydroxides have been studied by pH titration up to 95°C, as summarized by Schoonen (1994). Jayaweera et al. (1994) reported the zeta potential and $pH_{pzc}$ of a number of metal oxides, including rutile, hematite and magnetite, from streaming potential measurements at 235°C.

The stirred hydrogen electrode concentration cell (SHECC) design was developed at ORNL (Mesmer et al., 1970), and has been extensively applied to the determination of the equilibrium constants of protolytic reactions in homogeneous aqueous solutions (Mesmer et al., 1995; Wesolowski et al., 1995). Recently, we have developed a potentiometric method for studying $H^+/OH^-$ adsorption/desorption on mineral surfaces at temperatures to 295°C, by measurement of the solution pH during acid/base titrations of a suspension of the powdered mineral of interest as a function of temperature and ionic strength. The surface charge and $pH_{pzc}$ of rutile in 0.03–1.1 molal NaCl and tetramethylammonium chloride solutions have been well established by this approach (Machesky et al., 1994, 1998), and we have also investigated the sorption of $Ca^{2+}$ by rutile over a similar temperature range (Ridley et al., 1999). These initial studies were greatly facilitated by the extreme insolubility of rutile, even at extremes of pH, temperature and ionic strength, and the absence of strong specific counterion binding on the mineral surface in NaCl media. These studies confirm the trends observed over the more limited range of temperatures reported previously: (a) the $pH_{pzc}$ approximately parallels the temperature trend of $1/2\ pK_w$, where $K_w$ is the dissociation constant of water; (b) the proton-induced surface charge at a given ionic strength and pH, relative to the $pH_{pzc}$, increases with increasing temperature above the $pH_{pzc}$ due to the ability of solution cations to more effectively screen surface charge buildup as the dielectric constant of the medium decreases; and (c) interaction of solution cations with the surface becomes more specific with increasing temperature, in a direct analogy with ion pairing in solution. Chloride binding with the positively charged rutile surface was found to be more constant with temperature, although the accessible pH range investigated was more limited below the $pH_{pzc}$.

This communication presents the results of our ongoing studies of the surface charge of magnetite under hydrothermal conditions. Because magnetite is more soluble than rutile, particularly in mildly acidic solutions, and because $Fe^{2+}$ is known to form strong complexes with chloride (Heinrich and Seward, 1990; Palmer and Hyde, 1993), we chose to conduct these studies in sodium trifluoromethanesulfonate (NaTr or NaTriflate, with the chemical formula $NaCF_3SO_3$). Triflate is a synthetic, large, singly charged anion that has good thermal stability and has been shown to only weakly interact with cations in a number of

studies in this laboratory (cf. Palmer and Drummond, 1988; Wesolowski et al., 1998). It has been suggested that magnetite might reduce the $SO_3$ group of the Triflate anion. However, it is not apparent that magnetite would be any more effective as a reducing agent than $H_{2,g}$ in the presence of platinum black, and background titrations of the electrolyte in the absence of magnetite, used to correct the sorption isotherms as discussed below, incorporate any reduction of the electrolyte which might result in a change in pH.

## 2. Background

The surface charge on a mineral in contact with an aqueous solution arises from ''structural'' charge associated with the terminal oxygen atoms at the mineral surface that have unsatisfied valence, as well as ions from the solution which associate with these terminal oxygens and the underlying metal ions. Typically, water itself is the major agent involved in this interaction, undergoing dissociation and contributing $H^+$ and $OH^-$ ions which are strongly bound to surface sites. The general approach is to assume that these labile protons and/or hydroxyl groups reside at the mineral surface and experience the potential of the mineral surface, but are free to exchange with the solution (Stumm, 1992). The simplest description of this interaction is the ''one-p$K$ model'', wherein the surface is characterized by a single terminal charge-determining site which may exchange with protons from the solution according to

$$\equiv S^{-z} + H_s^+ \Leftrightarrow \equiv SH_s^{(1-z)} \quad (1)$$

where $z$ is a fractional charge usually less than or equal to unity, and $H_s^+$ signifies the activity of hydrogen ion at the surface. The concentrations of negatively and positively charged surface sites are then related through an equilibrium constant, $K_H$. This ''single site'' approach can also be formulated as a ''two-p$K$ model'':

$$\equiv S^- + H_s^+ \Leftrightarrow \equiv SH_s^\circ \quad (2)$$

$$\equiv SH_s^\circ + H_s^+ \Leftrightarrow \equiv SH_{2,s}^+ \quad (3)$$

The ''zero point of charge'' of metal oxides in contact with aqueous solutions is normally defined as the pH at which the surface sites and their associated bound protons and hydroxyl groups establish a zero net surface charge (e.g., where the concentration of $\equiv S^-$ equals the concentration of $\equiv SH_{2,s}^+$ for the two-p$K$ model). A generic term for this condition is the ''$pH_{pzc}$'' or point of zero charge. In the absence of specific binding of other solution ions, or nearly identical specific binding by the cation and anion of the electrolyte medium, the overall surface charge is exactly balanced by protonated and deprotonated surface sites, the electrical double layer (EDL) collapses, and the surface has no net charge in terms of long-range coulombic interactions with the solution. This condition can be termed the ''$pH_{ppzc}$'', or ''pristine point of zero charge'', which is equal to $\log K_H + \log\{|z|/(1-|z|)\}$ for reaction (1), or $1/2(\log K_{H1} + \log K_{H2})$ in reactions (2,3). In the ideal case where no protolytic impurities are present in either the solution or solid phase, and no additional unaccounted-for solution–solid interactions occur, the $pH_{ppzc}$ may coincide with the condition in which the measured pH of the bulk solution is exactly that computed from the thermodynamic properties of the bulk solution, (i.e., there are no ''excess'' or ''missing'' $H^+$ or $OH^-$ ions in solution). This condition is often referred to as the $pH_{znpc}$ or ''zero net proton condition'' (Sposito, 1998). Potentiometric titrations of a known quantity of solution in equilibrium with a known surface area of a mineral at a constant temperature and solution ionic strength thus provide a means of quantifying the equilibrium constants of reactions (1–3).

## 3. Materials and methods

### 3.1. Synthesis and characterization of solids

Various published recipes (Regazzoni et al., 1981; Cornell and Schwertmann, 1996; Dresco et al., 1999) were followed for the precipitation of magnetite by addition of strong base and an oxidant to ferrous iron solutions at temperatures of 90°C to 200°C. These products were found to be exceedingly fine grained (submicron), with high surface areas (13–18 $m^2/g$).

X-ray diffraction (XRD) analyses indicated that they were generally free of hematite, with the exception of the synthesis conducted at 200°C. However, thermogravimetric analysis (TGA) of the products demonstrated that they all contained a substantial component (ca. 20–50%) of ferric oxide, presumably in the form of maghemite ($\gamma$-$Fe_2O_3$), which is isostructural with magnetite and has a nearly identical XRD pattern. The material synthesized at 200°C contained a similar amount of $Fe_2O_3$, but in the form of hematite ($\alpha$-$Fe_2O_3$), rather than maghemite. Several literature sources suggest that freshly precipitated, submicron magnetite very readily oxidizes to maghemite, which may explain the failure of the low temperature approaches to produce a stable product suitable for further experimentation (cf. Tamaura and Tabata, 1990).

Because these synthetic approaches require precipitation from a concentrated base solution, extensive washing of the material is required before it can be used for surface titrations, which depend critically on detailed proton balancing. This washing step may provide the opportunity for oxidation, although Ar-purged water was used, and the washing was conducted by vacuum filtration under a stream of high purity argon. Preliminary surface titrations with these synthetic materials indicated that the surface charge density for a given pH was inversely proportional to the ferric oxide ($Fe_2O_3$) mole fraction in the solid. Commercial magnetite from Alfa Chemicals, Inc. (Johnson Mathey Puratronic, 99.997%, metals basis) was found by XRD and TGA analyses to contain ca. 20% of hematite $\pm$ maghemite. Although the preliminary surface titrations conducted with this solid were reproducible, the sorption isotherms were apparently affected by the presence of fully oxidized $Fe_2O_3$ as well.

In order to reduce these partially oxidized starting materials at elevated temperatures, they were heated in the presence of buffers that would poise the hydrogen fugacity within the stability field of magnetite. The most successful configuration utilized a standard Autoclave Engineers stainless steel 300 cc bolted-closure pressure vessel, housing a gold boat containing about 90 g of the iron oxide. Adjacent to the gold boat were placed four quartz tubes containing about 20 g of nickel metal powder, with the ends loosely packed with quartz wool. Ten grams of water were poured over the iron oxide charge just before sealing and heating the vessel for various lengths of time ranging from several days to 1 month at both 500°C and 600°C. In the presence of water vapor, the reactions that occur within the pressure vessel are:

$$Ni + H_2O_g \Leftrightarrow NiO + H_{2,g} \quad (4)$$

$$3(Fe_2O_3) + H_{2,g} \Leftrightarrow 2Fe_3O_4 + H_2O_g \quad (5)$$

The hydrogen fugacity imposed by the $Ni/NiO/H_2O$ buffer is well above that of the hematite/magnetite boundary and well below that of the magnetite/wustite boundary (Huebner, 1971) at all temperatures, including the low temperatures experienced during quenching of the reaction. Thus, 1 mol of Ni metal can convert 6 mol of iron in the form of hematite or maghemite to iron in the form of magnetite. That reaction (4) proceeded was evidenced by the green color of NiO apparent along the exposed reaction surfaces of the nickel metal powder when the vessel was opened. TGA and XRD analyses of the run products also demonstrated that reaction (5) proceeded to completion, after several days to a week at both temperatures.

The exceedingly fine-grained nature of the hydrothermally synthesized magnetite starting materials, and the difficulty of rinsing the products and assuring a high purity iron oxide, prompted us to use the Alfa Chemicals, Inc., reagent as the material of choice, after the high temperature treatment described above. Another factor was the assumption that a coarser-grained magnetite would be more likely to remain stable throughout the period needed to complete the surface titration studies, if the solid were routinely stored in a sealed container under high purity argon. Thus, several 90-g batches of Alfa Puratronic Fe(II)Fe(III) oxide (lot#21971, BET surface area 1.5 $m^2/g$) were treated at 500°C for 2 weeks, as described above. Subsequent tests demonstrated that all batches processed in this way exhibited similar characteristics in terms of grain size and morphology, surface area, TGA characteristics, XRD and X-ray photoelectron spectroscopy (XPS) spectra, and surface charge properties. Repeated surface area determinations were made on separate aliquots of this material by Micromeritics, using multipoint Kr BET specific surface area analysis, giving a value of $0.922 \pm 0.051$ $m^2/g$. This average surface area was used for all subsequent calculations.

Before treatment, the Alfa Puratronic starting material consisted of blocky aggregates of 20–50 μm size, composed of amorphous, submicron, individual grains (Fig. 1). XRD patterns of this material show sharp peaks for magnetite, and lesser amounts of hematite. TGA analysis in an oxygen stream indicated that the weight gain upon heating to 1010°C was 2.88%. Conversion of pure magnetite to pure hematite by addition of oxygen would result in a theoretical weight gain of 3.45%, indicating that the commercial product contains 17% $Fe_2O_3$, roughly consistent with the XRD pattern. After heating for 2 weeks at 500°C in the presence of $Ni/NiO/H_2O$, the reagent material remained in 20–50 μm aggregates, but as shown in Fig. 2, each individual submicron grain reconstituted into well-formed magnetite crystals, showing cubic, octahedral and dodecahedral faces, with sharp edges and corners, and distinct growth planes. The XRD pattern for this material shows no peaks other than those attributable to pure magnetite. TGA analysis gave a weight gain of 3.40%, indicating at least 98.5% magnetite. Several batches of Alfa starting material were reacted for longer times (up to 1 month) and at higher temperature (600°C), with no further increase in the apparent magnetite content. It is concluded that the material is in fact pure magnetite, and that the slight deficiency in weight gain can be attributed to either adsorbed water not removed during the TGA pretreatment process, or a systematic instrument bias.

The O1s XPS spectrum of this treated material (Fig. 3) is very similar to the spectrum of the mag-

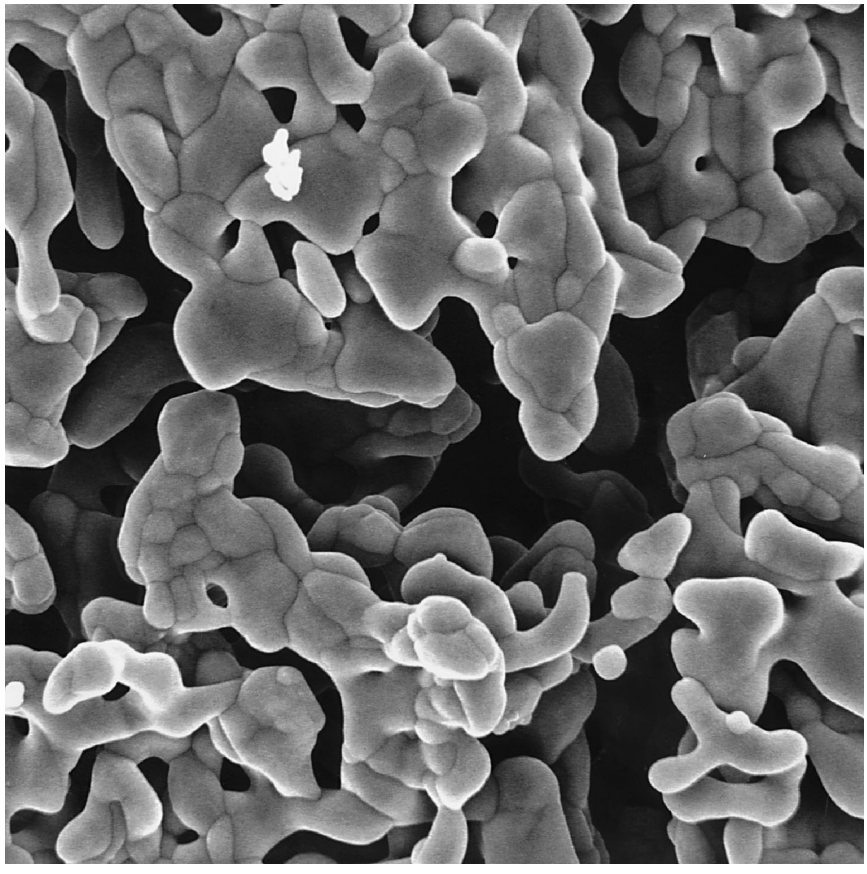

Fig. 1. SEM image of Alfa *AESAR* Puratronic (Johnson Matthey, 99.997%, lot#21971) Fe(II)/Fe(III) oxide, as received. The full frame is approximately 4.5 μm.

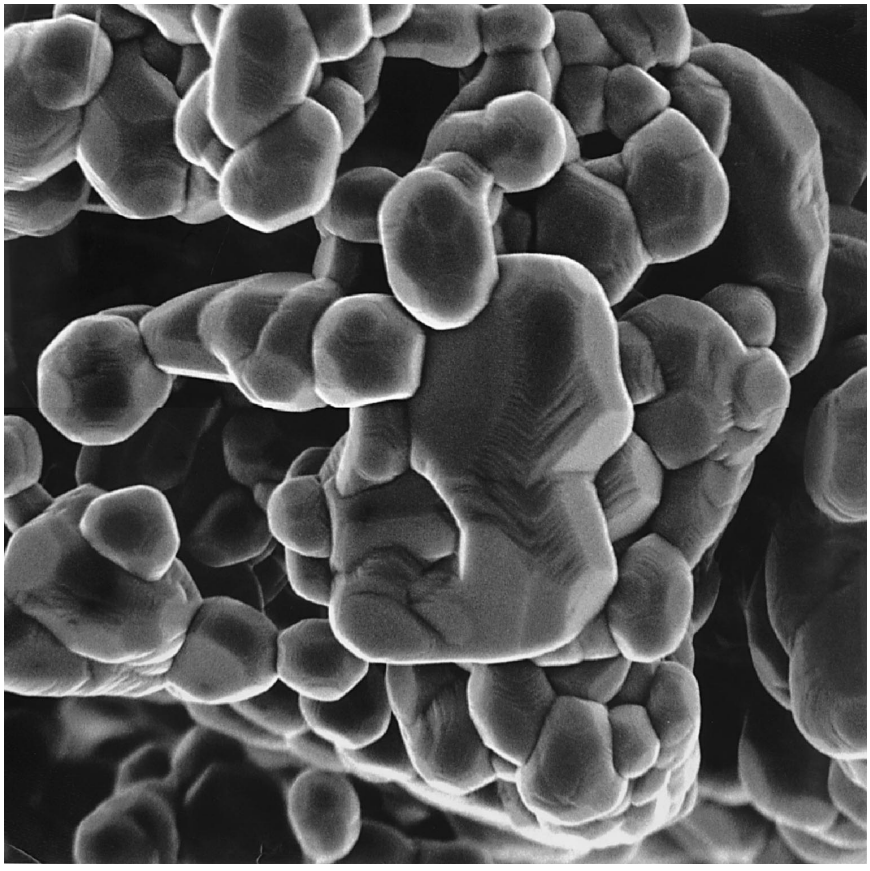

Fig. 2. SEM image of Alfa magnetite, lot#21971 treated at 500°C for 2 weeks with $Ni/NiO/H_2O$ (see text). Full frame is approximately 5 μm across. Note the distinct appearance of crystal faces (dodecahedral, cubic, and octahedral) and growth zones, as well as increased grain size, relative to Fig. 1.

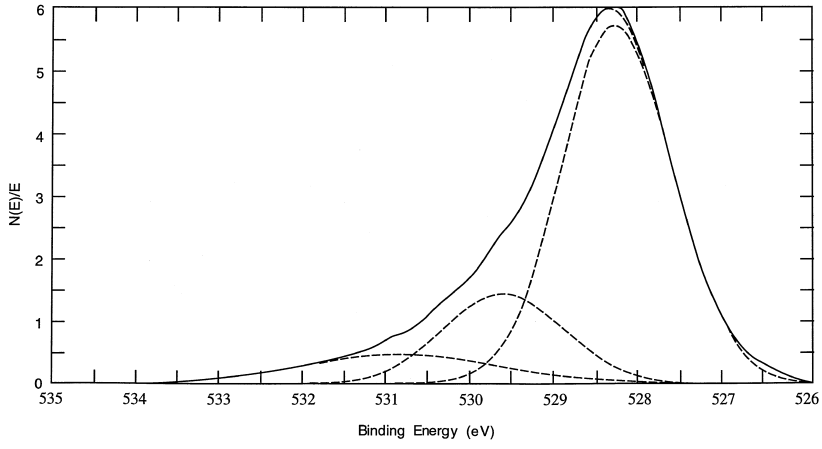


Fig. 3. XPS O1s spectrum of the treated Alfa magnetite of Fig. 2.

netite starting material used in the recent solubility studies of Ziemniak et al. (1995). Ar sputtering for up to 6 min revealed essentially no change in the O1s spectrum, indicating that the hydrated layer is relatively deep. This may reflect recrystallization in the presence of water vapor observed during the initial pretreatment. This is also consistent with the TGA results, where the total weight gain on oxidation is typically about 1.5% less than that expected from ideal magnetite. The presence of an extensive hydroxylated layer may also help rationalize the large negative surface charge densities (relative to the measured BET surface area) observed for this material, as will be discussed below. That is, this hydrated layer may allow penetration of the ''surface plane'' by $Na^+$, with the result that the measured BET surface area may underestimate the true reactive surface area. Analysis of the treated material after surface titrations in the SHECC at elevated temperature showed no change in the XRD pattern. Some increase in grain size may have occurred, but rinsing the samples before vacuum drying may have eluted some of the finer material. The O1s XPS spectrum of the material after surface titrations at 150°C and 200°C shows modest increases in the relative proportions of the two higher energy peaks, suggesting that these peaks represent adsorbed hydroxyl groups, as also suggested by Ziemniak et al. (1995).

Mössbauer spectra were obtained in the laboratories of Dr. J. Stucki at the University of Illinois and B. Moskowitz at the University of Minnesota on a number of our starting-material and run-product magnetite samples in order to confirm the TGA results. Both laboratories report that the material is essentially pure stoichiometric magnetite, with one third of the Fe in tetrahedral coordination and two thirds in octahedral coordination, with a ratio of octahedral to tetrahedral sites of 1.92:1. Magnetic saturation measurements at the University of Minnesota gave 90.9 A $m^2/g$ for the treated Alfa starting material, as compared with 90–92 A $m^2/g$ for ''pure'' magnetite, 65–75 A $m^2/g$ for maghemite and 2 A $m^2/g$ for hematite (B. Moskowitz, 1998, personal communication). ''Magnetite'' precipitated from highly basic aqueous solutions at low temperature, using the conventional synthesis method, gives saturation magnetizations of 84 A $m^2/g$ or less (Dresco et al., 1999), providing further evidence that such solids contain a significant maghemite component.

The Alfa Puratronic lot#21971 magnetite, pretreated at 500°C for 2 weeks under the $Ni/NiO/H_2O$ hydrogen fugacity buffer, was used for the bulk of the titrations presented below, and the modeling results apply to this material. Recently, we synthesized an additional batch of magnetite, using Alfa Puratronic lot#22387. However, this material was ground in an agate mill prior to heat treatment, which increased the surface area to approximately 4 $m^2/g$. This material was then reacted with $Ni/NiO/H_2O$ for 5 days at 500°C. The surface area after treatment decreased to $1.72 \pm 0.06$ $m^2/g$, nearly twice the surface area of the material used for the bulk of the experiments. Preliminary titration results with this new solid phase are also presented below.

### 3.2. Solution preparation

Large batches of HCl and NaOH (ca. 1 molal each) solutions are maintained in our laboratories and stored in polypropylene carboys under positive argon pressure. These solutions, prepared from reagent grade chemicals and distilled–deionized water (Barnstead NANOpure) are frequently standardized by titrations against ultrapure, vacuum dried potassium acid phthalate and sodium carbonate to better than 0.1%. The NaOH stock is prepared from 50% NaOH, which minimizes carbonate contamination. These stocks were diluted with deionized water as needed, by weight. Trifluoromethanesulfonic (''triflic'') acid was obtained from Kodak and purified by vacuum distillation. The sodium salt was prepared by neutralization of triflic acid with NaOH and recrystallized in ethanol as described by Palmer and Hyde (1993). From the purified triflic acid and sodium triflate, stock solutions of approximately 1 molal concentration were prepared. The acid solution was standardized by titration against our stock NaOH solution. The sodium salt solution was first acidified with a small amount of purified triflic acid, then sparged with high purity argon to remove $CO_2$, then neutralized by titration with NaOH under an argon flow. This solution was standardized by passing through a cation exchange column (DOWEX-50WX8-100) and titrating the acidic eluent with our stock NaOH solution.

### 3.3. Experimental methods and data reduction

The SHECC design and configuration used in this study have been described in a number of publications from this group (cf. Mesmer et al., 1970; Palmer and Hyde, 1993; Wesolowski et al., 1995, 1998). A typical SHECC is shown schematically, and the experimental procedure for surface titrations is described, in detail by Machesky et al. (1998). Approximately 1.5 g of magnetite powder were suspended in about 40 g of the test solution, which is stirred magnetically, as is a reference solution of known $H^+$ molality, connected to the test solution via a porous Teflon liquid junction. The cell is allowed to equilibrate overnight at temperature. After each addition of titrant to the test solution, a period of approximately 15–20 min elapses before recording the cell potential. During this time, the potential drift was generally observed to exponentially approach a stable value, reaching a drift rate of less than 0.1 mV/min, except at 25°C and 50°C. In this way, about 15–20 titrant aliquots were added, over a pH range of 6–7 units. At 25°C and 50°C, up to 2 days were required for initial equilibration (consumption of free oxygen by reaction with hydrogen at the electrode surfaces), and the potential after each titrant addition stabilized after several hours.

The cell configuration at the start of each experiment was

$$\underset{\text{test solution}}{H_2,Pt|NaTriflate(m_1),NaOH(m_2)}\,||\,\underset{\text{reference solution}}{NaTriflate(m_3),HTriflate(m_4)|Pt,H_2}$$

The ionic strengths of the two solutions were held as close to identical as possible, with $m_1 \approx m_3 \gg m_2 \approx m_4$ representing the stoichiometric molalities of the solution components. Typically, $m_2$ and $m_4$ were 0.001 molal at 0.03 molal ionic strength and 0.002 molal at 0.30 molal ionic strength. The titrant composition was typically 0.01 molal HTriflate with its ionic strength adjusted with NaTriflate such that the ionic strength of the test solution remained approximately constant throughout the titration (allowing for neutralization of $OH^-$ by $H^+$). An acidic reference was always employed, since it is known that Triflate is stable essentially indefinitely in acidic solutions over the temperature range of our studies (Fabes and Swaddle, 1975). The starting test solution was always basic in order to minimize dissolution of magnetite during the overnight equilibration and the bulk of the titration.

Each electrode responds to the half cell reaction $H_{2,g} \Leftrightarrow 2H^+_{aq} + 2e^-$. Since the hydrogen fugacity is constant over both solutions (the head spaces are interconnected), the potential between the electrodes is given by the Nernst equation

$$\Delta E = E_{test} - E_{ref} = -(RT/F)\ln(aH^+_{test}/aH^+_{ref}) + E_{lj} \quad (6)$$

where $R$ and $F$ are the gas and Faraday constants, $T$ is the temperature in K, and $E_{lj}$ is the liquid junction potential between the solutions. When the ionic strength of the test solution is nearly equal to that of the reference, and both are controlled by a ''swamping'' strong electrolyte, the concentration of which is at least an order of magnitude higher than all other reactants, the stoichiometric molal activity coefficients of $H^+$ can be reasonably assumed to cancel. The $pH_m \equiv -\log[H^+]$, with the brackets indicating stoichiometric molal concentration, of the test solution is then given by

$$pH_{m,test} = (F/2.3026RT)(\Delta E - E_{lj}) + pH_{m,ref} \quad (7)$$

As discussed by Mesmer and Holmes (1992), the Henderson equation (Baes and Mesmer, 1986, eq. 2-12) gives a reliable value of the liquid junction potential of such a cell, with an estimated uncertainty of $\pm 25\%$. For this calculation, values of the limiting equivalent conductances of $Na^+$, $H^+$ and $OH^-$ were taken from Quist and Marshall (1965), and $Triflate^-$ from Ho and Palmer (1995). In most of the experiments, the computed liquid junction potential was less than 1 mV, which corresponds to an uncertainty in the calculated $pH_{m,test}$ of less than 0.005 units.

The solution model typically employed in this laboratory assumes that strong electrolytes, including NaOH, NaTriflate, HTriflate, etc., are completely dissociated in aqueous solutions, at least up to 300°C along the liquid–vapor saturation surface, such that their stoichiometric molalities are independent of temperature, as discussed by Wesolowski et al. (1998). Presumably at the higher temperatures ion pairs such as NaOH° form in solution, but these are implicitly incorporated in the stoichiometric activity coefficients derived from this solution model. In

order to convert to the activity scale of pH for reporting the results of this study, we assumed that the stoichiometric molal activity coefficient of $H^+$ in the test solution could be approximated by

$$\gamma H^+ = (\gamma H^+ \gamma OH^-)^{1/2} = (a_w K_w / Q_w)^{1/2} \quad (8)$$

where $a_w$, $K_w$ and $Q_w$ are the activity, thermodynamic dissociation constant at infinite dilution, and stoichiometric molal dissociation constant, respectively of water in NaTriflate solutions (Palmer and Drummond, 1988) of the same stoichiometric molal ionic strength as the test solution. An equivalent approximation was made by Machesky et al. (1994, 1998) in presenting our rutile surface titration data in NaCl media. The activity of water is not known in NaTriflate solutions at elevated temperatures, and was assumed to be the same as in NaCl solutions of equal ionic strength and temperature (Archer, 1992).

During a surface titration, the expected $pH_m$ in the absence of the solid is calculated from the known solution compositions, and compared with the measured $pH_m$. Excess $H^+$ in solution is assumed to have arisen from the dissociation of protonated surface groups (or alternatively, the adsorption of $OH^-$ onto the surface). Conversely, $H^+$ ''missing'' from solution is assumed to have sorbed onto the mineral surface (or to have been neutralized by $OH^-$ released from the surface). The micromoles of ''excess'' or ''missing'' protons in the test solution at each point in the titration, divided by the total surface area of solid exposed to the experimental solution, is the quantity of interest in these experiments. In the absence of any side reactions, this can be converted to proton-induced surface charge density via the relationship

$$\sigma_H = (\text{''solution excess''}\ \mu\text{mols}\ H^+/m^2) * (-F) \quad (9)$$

where $\sigma_H$ is the proton-induced surface charge density in $C/m^2$ and F is the Faraday constant (0.096485 $C/\mu$equivalent). The negative sign in Eq. (9) indicates that excess $H^+$ in solution corresponds to a deficit on the mineral surface (or an excess of $OH^-$), giving a negative proton-induced surface charge. Likewise, a deficit of $H^+$ in solution, defined as a negative quantity in Eq. (9), results in a positive calculated surface charge.

The left-hand side of Eq. (9) only equates to the proton-induced surface charge density if no proton producing or consuming side reactions occur, and the solution composition in the test cell can be calculated with sufficient accuracy from the starting and titrant solution masses, compositions and the measured pH. Teflon and platinum surfaces of the cell might adsorb $H^+$ or $OH^-$, and the starting solutions might contain trace levels of protolytic impurities that contribute erroneously to the proton balance calculation. In our surface titration studies with rutile, it was found that such effects were trivial in the SHECC in NaCl solutions to 250°C. However, the larger surface area of the solid phase used in these experiments (17 $m^2/g$) helped minimize such effects, since the surface area appears in the denominator in Eq. (9). It is not practical to simply add more solid to the cell to increase the surface area, as stirring becomes inefficient if more than about 2 g of solid are placed in the cell, using our current configuration.

In our magnetite experiments, the solid phase had a relatively low surface area, $0.922 \pm 0.05$ $m^2/g$. Also, it is known that Triflate, which was used as the ''inert'' anion in order to avoid enhanced magnetite dissolution, slowly decomposes in basic solutions at elevated temperature (Fabes and Swaddle, 1975). Although we have used this anion in a large number of potentiometric studies in this laboratory (cf. Palmer and Hyde, 1993; Wesolowski et al., 1998), the surface titration measurements are quite sensitive to small errors in solution composition and minor protolytic impurities. Therefore, we conducted background titrations with similar test, reference and titrant solution compositions but with no magnetite in the cell, at each temperature and ionic strength, over the entire range of pH investigated in the magnetite titrations. The values of excess or missing $H^+$ in these background titrations at each temperature and ionic strength condition were expressed in molal concentration units, fitted to polynomial functions of $pH_m$, and used to correct the concentration of $H^+$ calculated from Eq. (7) in the equivalent magnetite-present experiments. This correction is also referred to as a ''solution blank'' correction in the literature. However, it should be noted that the platinum/$H_2$ electrode response is rigorously thermodynamic, reversible and Nernstian, and is not subject to

drift and other extrathermodynamic effects associated with glass electrodes, which have typically been employed in previous surface titration studies. In glass electrode studies, these electrode-related artifacts contribute significantly to the solution blank correction.

## 4. Results

### *4.1. General features of the proton sorption isotherms*

Potentiometric titrations with magnetite absent and present were conducted at ionic strengths of 0.03 and 0.30 molal in NaTriflate media at temperatures of 25°C, 50°C, 100°C, 150°C, 200°C, 250°C and 290°C, and the experimental results are listed in the Appendix. The background-corrected magnetite proton sorption isotherms are plotted at each temperature in Fig. 4a–g. As can be seen, duplicate titrations at 0.03 molal ionic strength at 100°C and 150°C demonstrate reasonable reproducibility, with somewhat poorer reproducibility at 50°C. Note also that the 50°C isotherms, and particularly the 25°C isotherms, are rather irregular compared with the higher temperature data. This can be attributed to several factors. The elevated solubility of magnetite in mildly acidic solutions at the lower temperatures, coupled with the long period of time required for equilibration after each titrant addition, may have contributed to this irregularity. If any time-related surface hydration or reconstitution processes are active, then they may have proceeded further at the lower temperatures due to the long initial equilibration time required. Also, the 25°C and 50°C isotherms exhibit downturns at the highest pHs, which may be an artifact of the extreme sensitivity of the computed excess $H^+$ in solution to the measured pH at these very high pHs.

All of the curves share some common features. At all temperatures studied, the curves at 0.30 molal ionic strength lie above those at 0.03 molal over the basic pH range, where the surface is expected to be negatively charged (excess $H^+$ in solution). This is a typical feature of proton sorption isotherms, which typically have slopes that steepen with increasing ionic strength due to the ability of solution cations and anions to electrically shield the buildup of negative or positive surface charge density, respectively. Fig. 5 shows plots of the isotherms at all temperatures, at 0.03 molal ionic strength and 0.30 molal ionic strength. As was observed in our studies of rutile surface protonation in NaCl media, the slopes of the curves at high pH increase with increasing temperature from 25°C to 250°C. Machesky et al. (1994, 1998) attributed this to closer approach of $Na^+$ to the surface with increasing temperature, due to a concomitant decrease in the dielectric constant of water, which weakens the strength of hydration water binding to the cation and/or the charged surface. At 290°C, the isotherms are clearly initially steeper than at 250°C, but quickly drop to a nearly flat plateau in the intermediate pH range, lying below the curves at 100–250°C. There are no data available for other solids with which to compare this behavior at this extreme temperature. The shapes of the sorption isotherms at 290°C could be attributed to more rapid reconstitution or recrystallization of the mineral surface at the highest temperature, resulting in fewer sorption sites and/or lower surface area, or could be related to decomposition of Triflate at the highest temperatures in an irreproducible way. An examination of the Appendix will show that the background correction in the intermediate pH range at this temperature is very large, relative to the uncorrected titration results.

All of the curves also exhibit a common intersection point ($pH_{cip}$) of the 0.30 and 0.03 molal isotherms at a low pH (except at 290°C where the isotherms still closely approach one another at low pH). This is also a typical feature of proton sorption isotherms, and in the absence of strong specific binding of solution counterions, and unaccounted-for protolytic side reactions, this has been interpreted as approximating the $pH_{pzc}$ of the surface. As discussed by Lyklema (1984) and Sposito (1998), however, these $pH_{cip}$ values are strongly influenced by specific binding by solution counterions and may differ in a predictable way from the $pH_{ppzc}$. In the case of magnetite in this study, the $pH_{cip}$ may also be influenced by a protolytic side reaction involving dissolution of magnetite. This is almost certainly the cause of the remaining common feature of the sorption isotherms, the sharp downturn to negative values of excess $H^+$ in solution, at pHs below the $pH_{cip}$ value.

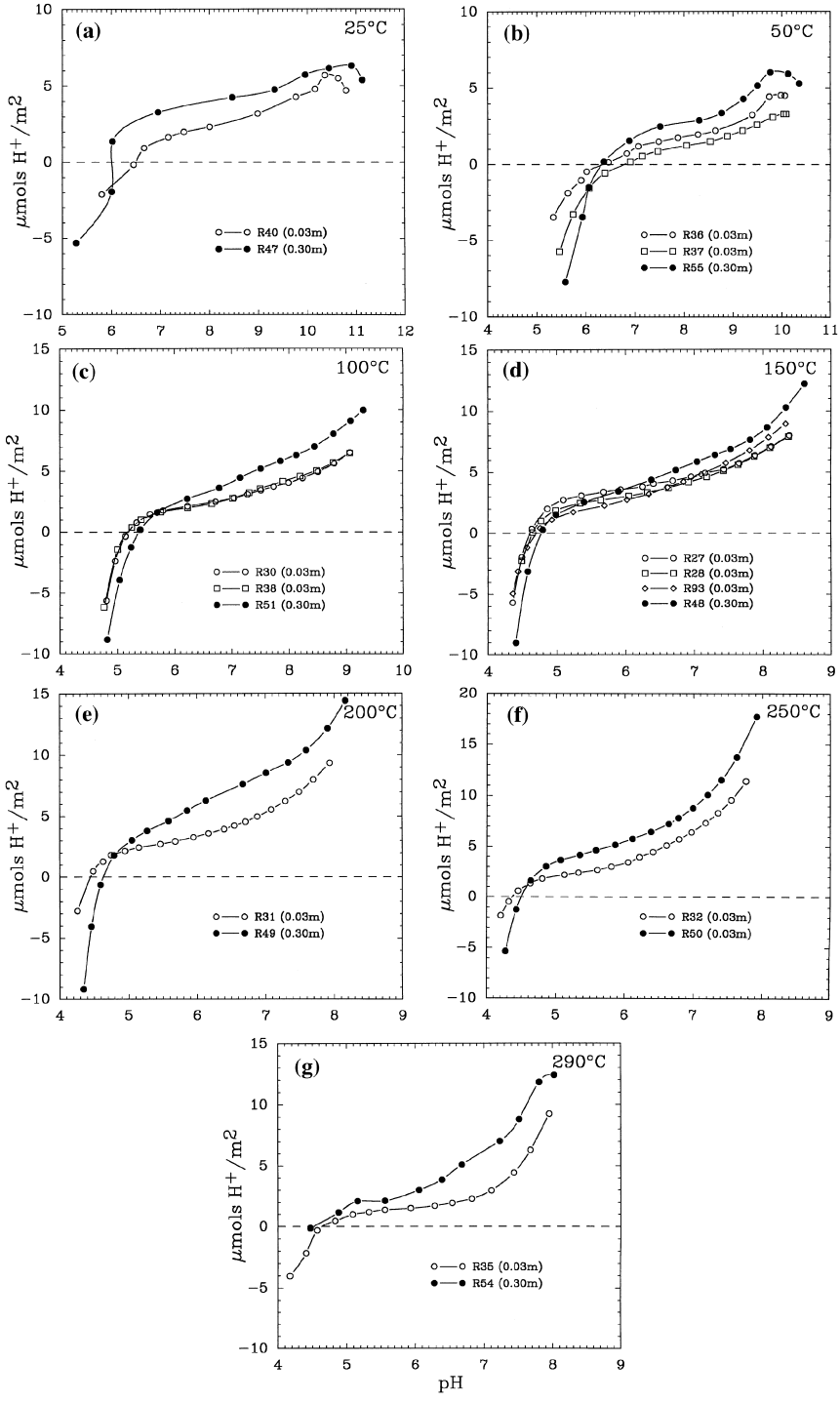


Fig. 4. Background-corrected proton sorption isotherms obtained from our experiments (Appendix) with treated Alfa magnetite in 0.03 and 0.3 molal NaTr at temperatures of 25°C (a), 50°C (b), 100°C (c), 150°C (d), 200°C (e), 250°C (f), and 290°C (g).

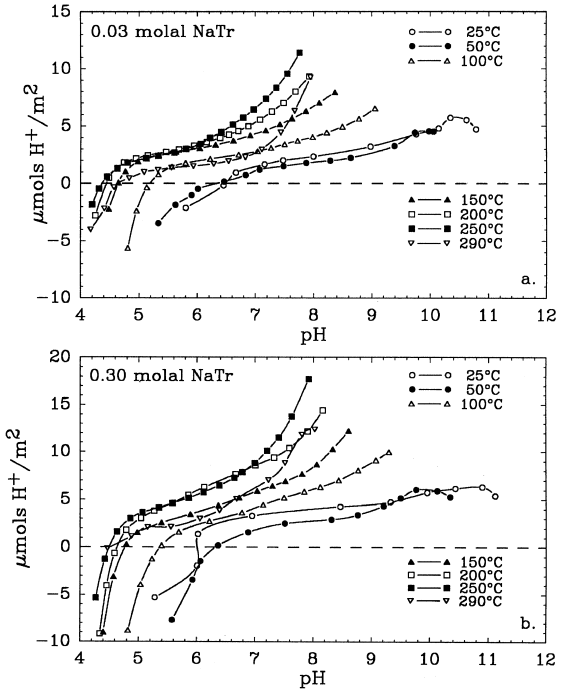


Fig. 5. Background-corrected proton sorption isotherms (Appendix) as a function of temperature in 0.03 molal NaTr (a) and 0.30 molal NaTr (b).

In order to substantiate this last point, surface titrations were conducted with identical solutions and solid loadings as the 0.03 molal titrations at 100°C, 150°C, 200°C and 250°C, but with samples removed for analysis of the total Fe content at selected pHs. Samples were withdrawn from the test compartment through a platinum dip tube, as described by Palmer et al. (2000). The acidified samples greater than 100 ppb ΣFe were analyzed for total iron by ICP using a Thermo Jarrell Ash IRIS instrument, and by graphite furnace AA for samples in the 1–100 ppb range, using a Perkin Elmer 4110 ZL spectrometer. Precision of total iron analyses was 1–2% at concentrations above 10 ppb, and 10–20% at lower concentrations.

### *4.2. Magnetite dissolution effects*

Sampling disturbs the solution mass balance, particularly for this low-surface area material, and so the computed proton sorption isotherms are not well matched to the isotherms obtained with no sampling. However, we attempted to duplicate the length of time between titration points and the overall time from the initiation of the experiment, in order to correct the isotherms in Fig. 4 for the dissolution reaction, which is a proton-consuming reaction. Over most of the pH range, the total iron in solution was found to be near or below our detection limits (about 0.1 ppb), consistent with the magnetite solubility model of Ziemniak et al. (1995), which is in good agreement with the earlier work of Tremaine and LeBlanc (1980). At these levels, there is insufficient iron in solution to significantly affect the computed excess $H^+$ in solution. However, substantial iron concentrations were detected at pHs below the $pH_{cip}$ values in Fig. 4 as shown in Fig. 6a–d.

The experimentally determined iron concentrations are shown as diamonds in Fig. 6. The smooth curves correspond to model calculations of the iron concentration in solution for the dissolution of magnetite controlled by two possible reactions:

$$1/3Fe_3O_4 + 2H^+ + 1/3H_2 \Leftrightarrow Fe^{2+} + 4/3H_2O \quad (10)$$

$$Fe_3O_4 + 2H^+ \Leftrightarrow Fe_2O_{3(\text{hematite})} + Fe^{2+} + H_2O \quad (11)$$

The equilibrium constants for these reactions were computed from the solubility and speciation models of Ziemniak et al. (1995, solid curves in Fig. 6) and Shock et al. (1997, dashed curves in Fig. 6). For these calculations, we assumed that the partial pressure of $H_2$ was 10 bars at the experimental temperature, and that the ionic strength dependence of the molal equilibrium quotients of reactions (10 and 11) was the same as for the dissolution of ZnO in acidic NaTriflate solutions of the same temperature and ionic strength (Wesolowski et al., 1998), which involves the same charge types. The hydrogen partial pressure was converted to fugacity using an equation of state for $H_2$–$H_2O$ mixtures (Ely and Huber, 1990), although this is a minor correction term. The variation of hydrogen partial pressure from one experiment to another was no more than a factor of two to three, which would result in a change in the equilibrium concentration of $Fe^{2+}$ by 0.1–0.2 log units for reaction (10), while reaction (11) is redox independent. Other aqueous iron species were also considered in the calculation, including the hydrolysis species of Fe(II) and Fe(III), and it was assumed that

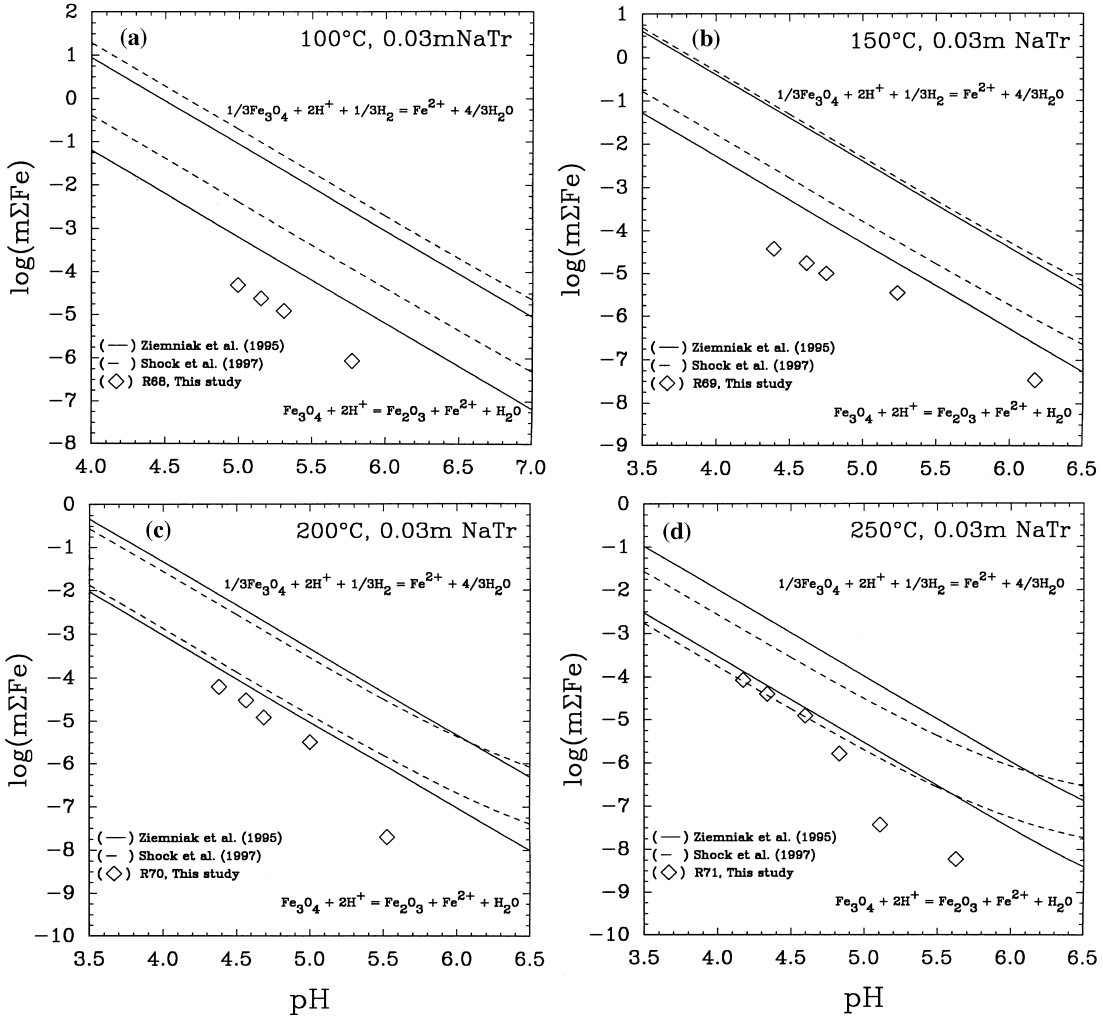


Fig. 6. Sampling runs at 100°C (a), 150°C (b), 200°C (c) and 250°C (d) in 0.03 molal NaTr, in which samples were withdrawn for total iron analysis. The solid lines are the solubilities computed from the model of Ziemniak et al. (1995) and the dashed curves from the model of Shock et al. (1997), for reaction (10, upper two curves) and reaction (11, lower two curves).

redox equilibrium was attained among the aqueous iron species. These calculations indicate that at the conditions of our studies $Fe^{2+}$ is the dominant dissolved iron species, with significant amounts of $Fe(OH)^{2+}$ appearing only at the highest temperatures and pHs.

Under the hydrogen fugacity conditions of our experiments, hematite is thermodynamically unstable by many orders of magnitude, and reaction (10) should control the equilibrium solubility of iron. However, in unpublished experimental studies of magnetite solubility in NaTriflate solutions containing 0.01–0.0001 molal Htriflate, using the SHECC cell in a similar manner to our studies of ZnO solubility (Wesolowski et al., 1998), we found that magnetite was partially or entirely converted to well-crystallized hematite over a period of hours to days, even at $H_2$ partial pressures of 10–50 bars, at temperatures of 100–250°C. We believe that the active process is kinetically controlled leaching of Fe(II) out of the magnetite lattice, leaving maghemite which then recrystallizes at temperatures above about

100°C to hematite. This type of behavior has been reported by other authors under anoxic conditions, but with no strong reducing agents present (Swaddle and Oltmann, 1980; Jolivet and Tronc, 1988; White et al., 1994). In longer-term experiments in our laboratories, we appear to have been able to obtain reversible solubility products for reaction (11) at 150°C and 200°C, which are in fairly good agreement with the models of Ziemniak et al. (1995) and Shock et al. (1997).

As shown in Fig. 6, it is clear that at 100°C the measured total iron in solution falls more than three orders of magnitude below the level predicted by either model for reaction (10), and more than an order of magnitude below that of reaction (11). However, at the lowest pHs, the stoichiometry of reactions (10, 11), which dictate a −2 slope of log$\Sigma$Fe vs. pH when $Fe^{2+}$ is the dominant species in solution, is approached at all temperatures. Furthermore, the measured total iron levels at the highest temperatures and lowest pHs closely approach the total iron content predicted from reaction (11), while remaining orders of magnitude below the levels predicted for reaction (10). Analyses of run products from several surface titrations did not demonstrate the presence of hematite, but only minute amounts of hematite need be formed via reaction (11) to account for the total iron content of the experimental solutions. It appears likely that over the time frame of our surface titrations, and even in our longer-term solubility studies in the SHECC, the solutions are approaching a reversible metastable equilibrium involving reaction (11), but are kinetically hindered from approaching saturation, even with respect to this metastable reaction, at the lower temperatures and higher pHs.

In order to apply a correction for this proton-consuming reaction to the sorption isotherms, regression equations were fitted to the measured total iron concentration vs. measured molality of $H^+$ for the three lowest-pH samples at each temperature in Fig. 6, assuming that the measured iron in solution was all in the form of $Fe^{2+}$ and that two $H^+$ ions were consumed for each $Fe^{2+}$ ion in solution. This would represent the maximum correction factor, as the first and second hydrolysis species of $Fe^{2+}$ would consume either one or zero $H^+$ ions for each iron species released to solution. As can be seen in Fig. 7a–d, application of this solubility correction factor appears to essentially eliminate the sharp downturn in the sorption isotherm at 100°C, has a nearly negligible effect at 150°C, and overcorrects the isotherms at 200°C and 250°C.

The apparent observation that the level of dissolved iron in our experiments is kinetically controlled by a metastable mineral assemblage may explain why the correction factors obtained from the sampling experiments did not uniformly improve the sorption isotherms. It is very difficult to exactly match the time of exposure of magnetite to the solution at a given pH from the sorption experiments

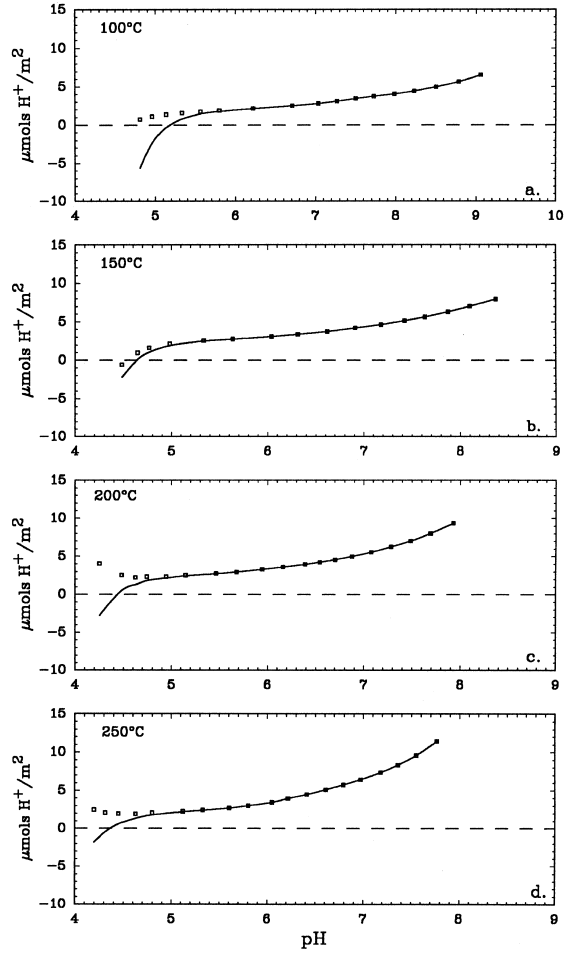


Fig. 7. Proton sorption isotherms in 0.03 molal NaTr (Fig. 4 and Appendix) corrected for magnetite dissolution effects (open squares) at (a) 100°C, (b) 150°C, (c) 200°C and (d) 250°C, compared with uncorrected curves from Fig. 4 (solid curves).

to the sampling runs. However, the most important observation, apparent in Fig. 7, is that this correction, regardless of whether it is too large or too small for a given isotherm, has virtually no effect on the sorption isotherms at pHs above the $pH_{cip}$. We did not conduct solubility measurements in the 0.30 molal solutions, and the positions of the $pH_{cip}$ values relative to the shape of the 0.30 molal isotherms suggests that dissolution may have affected these isotherms to pHs slightly above the $pH_{cip}$. However, it can be reasonably demonstrated that dissolution of magnetite has little or no influence on the shape of the sorption isotherms over most of the pH range studied.

Because of the extreme uncertainty associated with the solubility correction, the fact that we did not obtain such data at other ionic strengths or temperatures, and the fact that the correction only affects the last few points in each titration, we chose to ignore this correction in modeling the results of this study. We conclude from these observations that little useful information can be obtained about the proton binding and surface charge behavior of magnetite at pHs below the observed $pH_{cip}$ values. Fortunately, these pHs are more acidic than the neutral pH, and many naturally occurring solutions are buffered at higher pHs. Furthermore, our studies with rutile demonstrate that shielding of positive charge and specific ion binding by solution anions is much weaker than that of cation interactions with negatively charged surfaces (Machesky et al., 1998), at least for NaCl, the most abundant salt in natural waters. Finally, cation interactions with negatively charged surfaces are more directly useful in studies of trace element, contaminant, and ore metal mobilities in subsurface environments.

## 5. Discussion

At 0.30 molal ionic strength, only one set of isotherms were obtained. To simplify the discussion and modeling that follows, we have chosen to select representative sorption isotherms from the duplicate runs at 0.03 molal ionic strength, namely runs 36, 30 and 28 at 50°C, 100°C and 150°C, respectively (Fig. 4). The 25°C isotherms at both ionic strengths exhibit highly irregular shapes, compared with the results at other temperatures. Furthermore, unlike the other temperatures studied, the $pH_{cip}$ occurs at a significantly negative value of ''excess'' $H^+$ in solution. We will not include these 25°C results in the following discussion and model development.

### 5.1. Estimates of the magnetite zero point of charge

Published literature values for the $pH_{pzc}$ of magnetite as a function of temperature are plotted in Fig. 8, along with the theoretically predicted 25°C value of Sverjensky and Sahai (1996). These and a number of other published estimates at 25°C are listed in Table 1. Tewari and McLean (1972) and Blesa et al. (1984) performed pH titrations of magnetite surfaces

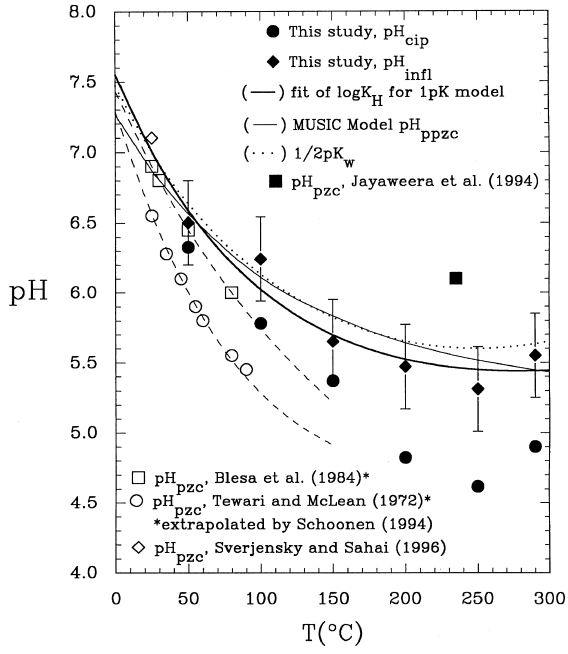


Fig. 8. Estimates of the point of zero charge of magnetite from this study and the literature as a function of temperature, including $pH_{cip}$ and $pH_{infl}$ values from our study, together with the fit to the $pH_{infl}$ values represented by Eq. (13). Also shown are the published experimental values of $pH_{pzc}$ reported by Blesa et al. (1984) and Tewari and McLean (1972), along with the empirical extrapolations of those literature results reported by Schoonen (1994), and the model estimate at 25°C of Sverjensky and Sahai (1996). The value $1/2pK_w$ for the dissociation of water (Busey and Mesmer, 1978) and the $pH_{ppzc}$ values calculated from the extended MUSIC model are also shown as discussed in the text. The point of zero charge estimate from the streaming potential studies of Jayaweera et al. (1994) at 235°C is also shown.

Table 1
Selected published values of the $pH_{pzc}$ of magnetite obtained from pH titration and electrophoretic mobility measurements, as well as theoretical estimates

| $T$ (°C) | $pH_{pzc}$ | Reference |
|---|---|---|
| 25 | 8.2 | Shen et al. (1999), titration[a] |
| 25 | 5.55 | Catalette et al. (1998), titration[b] |
| 25 | 6.3 | Marmier et al. (1999), titration[c] |
| 25 | 7.1 | Sverjensky and Sahai (1996), triple layer model |
| 25 | 6.5 | Parks (1965), mobility |
| 30 | 6.8 | Regazzoni et al. (1983), titration |
| 25 | 6.85 | Regazzoni et al. (1983), mobility |
| 25 | 6.90 | Blesa et al. (1984), titration |
| 30 | 6.80 | Blesa et al. (1984), titration |
| 50 | 6.45 | Blesa et al. (1984), titration |
| 80 | 6.00 | Blesa et al. (1984), titration |
| 25 | 6.55 | Tewari and McLean (1972), titration and addition[d] |
| 35 | 6.3 | Tewari and McLean (1972), titration and addition |
| 45 | 6.1 | Tewari and McLean (1972), titration and addition |
| 55 | 5.9 | Tewari and McLean (1972), titration and addition |
| 60 | 5.8 | Tewari and McLean (1972), titration and addition |
| 80 | 5.6 | Tewari and McLean (1972), titration and addition |
| 90 | 5.4 | Tewari and McLean (1972), titration and addition |

[a] No discussion in this reference of precautions taken to avoid oxidation of the ultrafine ''magnetite'' used, nor is the presence of magnetite confirmed.

[b] Authors suggest that $pH_{pzc}$ of natural magnetite used may be affected by silica impurity.

[c] Same starting material as used in this study, but without $Ni/NiO/H_2O$ pretreatment.

[d] pH titration and ''oxide addition'' methods used. Values between 25°C and 90°C interpolated from a figure in the reference.

to 90°C and 80°C, respectively. Schoonen (1994) extrapolated these experimental results into the hydrothermal regime using an empirical, isocoulombic approximation method, and these extrapolations are also shown in Fig. 8. Schoonen gives equations for use to 150°C, but states that the propagation of errors makes these estimates highly uncertain above this temperature. Jayaweera et al. (1994) used a yttria-stablized zirconia pH sensor and external $Pt/H_2$ reference electrode to perform streaming potential measurements at 235°C on a number of oxide phases, including magnetite, for which they report a $pH_{pzc}$ of 6.1.

The magnetite used in the study of Tewari and McLean (1972) was precipitated by titrating ferrous sulfate into an $NaOH + KNO_3$ solution. Emission spectrographic and XRD analyses were performed on this solid material, but neither method can effectively distinguish between magnetite and maghemite. Blesa et al. (1984) prepared their solid by reacting a slurry of ferrous hydrous oxide with nitrate in the presence of hydrazine, which they found beneficial in minimizing the formation of maghemite during the oxidative precipitation reaction. In addition to XRD analysis, they comfirmed that the solid phase was fairly pure magnetite by performing Mössbauer spectrometry as well as electrochemical measurements of the Fe(II)/Fe(III) ratio, as described in detail by Regazzoni et al. (1981). Jayaweera et al. (1994) do not provide details of the synthesis of the magnetite used in their study. Tewari and McLean (1972) report that no iron was observed (detection limit 55 ppb) in solutions sampled at the end of several of their titrations, although they indicate that solubility effects at the higher temperatures may have caused their titration results to be more scattered and to differ from experiments in which a known mass of magnetite was quickly added at temperature to a solution already at that temperature. Blesa et al. (1984) do not discuss dissolution effects, although they used a ''fast titration'' method, which may have minimized dissolution. The streaming potential measurements of Jayaweera et al. (1994) do not depend on solution proton balance calculations, and are therefore presumably not affected by dissolution of the solid, unless this significantly alters the pH of the output solution, or if these dissolved iron species readsorb to the magnetite surface.

Our $pH_{cip}$ values (Fig. 8, Table 2) are in good agreement with the reported $pH_{pzc}$ values of Blesa et al. (1984) and with Schoonen's extrapolation to 150°C. However, examination of Fig. 4 and the shapes of the 0.30 molal isotherms, in light of the magnetite dissolution effects observed in our 0.03 molal solutions, suggests that our $pH_{cip}$ values may be influenced by dissolution artifacts. Also, as will be discussed below, the relative steepness and asymmetry of the isotherms at higher pHs can only be adequately modeled by invoking strong specific binding of $Na^+$ at the mineral surface. Such specific cation binding, in the absence of compensatory binding by anions, causes the $pH_{cip}$ value to shift to a significantly lower pH than the $pH_{ppzc}$ (Lyklema, 1984; Stumm, 1992). Because of these competing effects, we suggest that the $pH_{cip}$ values observed in

Table 2
Values of the $pH_{cip}$ observed for magnetite sorption isotherms obtained in 0.03 and 0.30 molal NaTr, the $pH_{infl}$ values obtained from the 0.03 molal NaTr isotherms, and values of $\log K_H$ for the one-p$K$ model calculated from Eq. (13)

| $T$ (°C) | $pH_{cip}$ | $pH_{infl}$ | $\log K_H$ |
|---|---|---|---|
| 0 | | | 7.55 |
| 25 | | | 7.00 |
| 50 | 6.33 | 6.50 | 6.59 |
| 100 | 5.78 | 6.24 | 6.02 |
| 150 | 5.37 | 5.65 | 5.70 |
| 200 | 4.82 | 5.47 | 5.52 |
| 250 | 4.62 | 5.31 | 5.45 |
| 290 | 4.90[a] | 5.55 | 5.44 |
| 300 | | | 5.44 |

[a]Distance of closest approach of 0.03 and 0.30 molal isotherms(Fig. 4g).

this study may not accurately reflect the $pH_{ppzc}$ of the magnetite surface.

We therefore examined the isotherms in more detail, particularly those at 0.03 molal ionic strength, for other features that might better indicate the $pH_{ppzc}$. The 0.03 molal isotherms were fitted with polynomial functions and differentiated with respect to pH. Fig. 9 is a unitless derivative plot of a typical isotherm, for run #28 at 150°C and 0.03 molal ionic strength. As can be seen, there is a distinct minimum in the plot, indicating an inflection point ($pH_{infl}$) in the sorption isotherm at a pH of 5.65, somewhat higher than the $pH_{cip}$ value of 5.39. The 0.03 molal isotherms selected for modeling were all differentiated in this manner and the resulting $pH_{infl}$ values are plotted in Fig. 8, and listed in Table 2. Such inflection points are also predicted at the $pH_{ppzc}$ by the one-p$K$ surface charging model, although attempts to extract $\log K_H$ values simply by fitting the observed isotherms with this as an adjustable parameter proved unsuccessful, due to covariance with the other model parameters described below. Because of the strong cation binding apparent from the modeling effort, it is suggested that the $pH_{infl}$ values might give a better estimate of the $pH_{ppzc}$ of the magnetite surface. An uncertainty of $\pm 0.30$ log units is arbitrarily assigned to these estimates of the $pH_{ppzc}$, consistent with the maximum uncertainty in the $pH_{pzc}$ estimates for rutile (Machesky et al., 1998).

As can be seen, the $pH_{infl}$ values closely parallel the value of $1/2\ pK_w$ as was also demonstrated for the $pH_{pzc}$ of rutile to 295°C (Machesky et al., 1998). Also, the $pH_{cip}$ values deviate from the $pH_{infl} \cong pH_{ppzc}$ values increasingly with increasing temperature, which would also be predicted if specific binding of $Na^+$ with the negatively charged surface became stronger with increasing temperature. The $pH_{pzc}$ value reported by Jayaweera et al. (1994) from streaming potential measurements of the isoelectric pH at 235°C is higher than the $pH_{infl}$ values from this study. This is also consistent with strong cation binding, since the $pH_{cip}$ and $pH_{iep}$ values shift in opposite directions relative to the $pH_{ppzc}$ when specific cation binding is uncompensated by equivalent anion binding of the supporting electrolyte (Stumm, 1992). However, it should be noted that Jayaweera's estimate for the $pH_{pzc}$ of rutile at 235°C (6.6), is much higher than our estimate ($4.25 \pm 0.2$, Machesky et al., 1998).

### 5.1.1. One-pK model estimate

For rutile the simple one-p$K$ model for surface protonation was assumed (Bolt and Van Riemsdijk, 1982; Machesky et al., 1998),

$$-\mathrm{TiOH}^{-1/2}_{\mathrm{surface}} + \mathrm{H}^+_s \Leftrightarrow -\mathrm{TiOH}^{+1/2}_{2\,\mathrm{surface}}$$

$$K_{\mathrm{H,rutile}} = \left[\mathrm{TiOH}^{+1/2}_{2\,\mathrm{surface}}\right] / \left(\left[\mathrm{TiOH}^{-1/2}_{\mathrm{surface}}\right] \times \{\mathrm{H}^+\}_b \exp(-z_H F\Psi_o/RT)\right) \quad (12)$$

The $K_H$ expression in reaction (12) assumes that the activity coefficient ratio of the surface species is

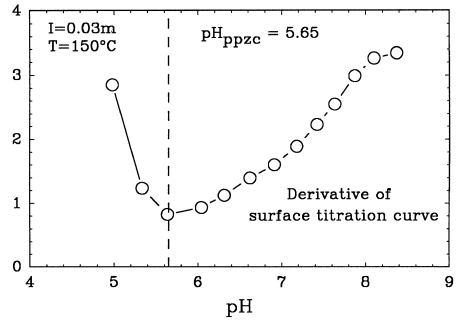


Fig. 9. Dimensionless plot of the derivative of a portion of the 150°C, 0.03 molal NaTr, background-corrected magnetite surface sorption isotherm for run #28 (Fig. 4d), showing the minimum in the curve ($pH_{infl}$) that was used as an estimate of the $pH_{ppzc}$ value.

unity, $z_H$ is the proton charge, $\Psi_o$ is the potential at the mineral surface, $F$ and $R$ are the Faraday and gas constants, respectively, and $T$ is the absolute temperature. The activity of the hydrogen ion in the bulk solution, $\{H^+\}_b$, was calculated from the measured molality of $H^+$ using activity coefficients defined in Eq. (8). Since $\Psi_o$ is zero at the $pH_{ppzc}$, and the concentrations of the positive and negative surface species are equal, $\log K_H = pH_{ppzc}$ for the one-p$K$ model with symmetrically charged surface species.

In the case of rutile, the $pH_{cip}$ occurred at nearly zero μmol excess $H^+/m^2$, and it was assumed that $pH_{ppzc} = pH_{cip.}$ Since dissolution of rutile is known to be insignificant in terms of the proton balance in solution, this suggests that specific cation and anion binding in the vicinity of the $pH_{cip}$ are weak and/or compensatory. Assuming that an equivalent one-p$K$ model could adequately represent the surface protonation of magnetite, the $pH_{infl}$ values can be equated to a one-p$K$ protonation constant, which then can be fit to a temperature function from which thermodynamic properties of the protonation reaction can be derived. The $pH_{infl}$ values from this study could be adequately fit with a constant heat capacity model, giving

$$\begin{aligned} pH_{infl} &\approx \log K_{H,magnetite} \\ &= -\left[\Delta H_{298}^\circ - 298\Delta C_p\right]/[2.303RT] \\ &\quad + \left[\Delta S_{298}^\circ - \Delta C_p(1+\ln 298)\right]/[2.303R] \\ &\quad + \Delta C_p \ln T/[2.303R] \end{aligned} \tag{13}$$

In order to better constrain the fit, the value of $\Delta S_{298}^\circ$ was fixed at 25.5 J $K^{-1}$ $mol^{-1}$, the best fit value for the equivalent rutile protonation reaction (Machesky et al., 1998), since presumably, the entropy of protonation, mainly related to loss of hydration waters on the $H^+$ aqueous species, would be similar for all metal oxides (Fokkink, 1987). The resulting best-fit thermodynamic parameters are $\Delta H_{298}^\circ = -32.4 \pm 0.8$ kJ/mol, $\Delta C_p = 128 \pm 16$ J $K^{-1}$ $mol^{-1}$, and $\log K_{H,298} = 7.00$. The values of $\log K_H$ from Eq. (13) are plotted in Fig. 8 and shown to be in good agreement with the $pH_{pzc}$ estimates of Blesa et al. (1984) to 80°C (6.90 at 25°C), as well as the theoretical prediction of Sverjensky and Sahai (1996) at 25°C of 7.1 from their ''triple layer'' model calculations. Values of $\log K_H$ calculated from Eq. (13) are listed in Table 2.

Sverjensky and Sahai (1998) have examined in detail the temperature dependence of surface protonation reactions reported in the literature, as well as direct measurements of the enthalpy of surface protonation. They have recast the literature data in terms of a single-site, two-p$K$ model, similar to reactions (2,3) above, with a ''triple layer'' EDL structure. With this model, the $pH_{pzc}$ is defined by the overall protonation reaction

$$\equiv S^- + 2H_s^+ \Leftrightarrow \equiv SH_{2,s}^+ \tag{14}$$

Thermodynamically, this is equivalent to reaction (12) with the thermodynamic constants ($\log K_H$, $\Delta H$, etc.) multiplied by two (Sverjensky and Sahai define the equilibrium constant for reaction (14) as $K_{zpc}$, such that their $pH_{zpc} = 1/2\log K_{zpc}$). From the data of Blesa et al. (1984), Sverjensky and Sahai (1998) extracted a 25°C enthalpy of protonation of −32.9 kJ/mol, in excellent agreement with the value determined from Eq. (13), whereas, from the data of Tewari and McLean (1972), a somewhat more negative value of −37.1 kJ/mol is reported, and their semi-empirical model for surface protonation gives a 25°C enthalpy of protonation of −36.8 kJ/mol.

### *5.1.2. MUlti-SIte Complexation (MUSIC) model estimate*

Both the one-p$K$ and two-p$K$ models (Eqs. 1–3) are obviously thermodynamic simplifications of what may be a very complex set of reactions and species at the molecular level. Furthermore, unlike rutile, magnetite possesses several distinctly different cation–oxygen structural configurations, including surface oxygens in both octahedral coordination with Fe(II) and Fe(III), and tetrahedral coordination with Fe(III), with site densities which differ from one crystal face to another. The MUSIC model approach of Hiemstra et al. (1989, 1996) specifically addresses the crystal structure of minerals, and predicts the proton binding constants for a variety of terminal oxygen sites, with oxygen bonded to one, two or three underlying metal ions. All of these contribute

to the $pH_{ppzc}$, the charging of the surface as a function of pH, and the interaction of the charged surface sites with electrolyte ions. The model is appealing, in that the proton binding constants are predicted from an independent empirical model based on the Pauling bond–valence principle (Hiemstra et al., 1989). In this sense, the MUSIC model uses a basis for estimating proton binding constants similar to that of Sverjensky and Sahai (1996). According to the refined MUSIC model (Hiemstra et al., 1996), surface protonation constants ($K_{Hy}$) can be estimated using the empirical relationship,

$$\log K_{Hy} = -A^{25°C}\left(V + \sum s_{Me-O} + m(s_H) + n(1 - s_H)\right) \quad (15)$$

where $A^{25°C}$ is the slope obtained from regression of a large number of $\log K$ values for homogeneous protonation reactions of oxygen-bearing aqueous species at 25°C, vs. the undersaturation of charge on the oxygen ligand. Again, this approach is related to the Born solvation model employed by Sverjensky and Sahai (1996, 1998) for the interaction of aqueous spieces with the mineral surface, since the Born solvation model has been demonstrated to rationalize the observed behavior of ions in aqueous media (cf. Shock et al., 1997). In Eq. (15), $V$ is the valence of oxygen ($-2.0$), $\sum s_{Me-O}$ is the sum (one, two or three for single, double or triple coordination, respectively) of the bond valence values for the metal–oxygen bonds (Me–O) of interest, $m$ is the number of donating H-bridges with adsorbed water (requires the presence of an H atom in the deprotonated, negatively charged species), $s_H$ is the bond valence of an adsorbed proton ($+0.8$), and $n$ is the number of accepting H-bridges with adsorbed water. For singly coordinated surface oxygens $(m + n) = 2$, for doubly coordinated surface oxygens $(m + n) = 1$ or 2, and for triply coordinated surface oxygens $(m + n) = 1$.

The atomic configuration of the magnetite surface as envisioned by Jolivet and Hernandez (1999) was used to estimate the coordination and bond lengths of the terminal oxygens, as well as the site charges and densities. This unpublished manuscript, which utilizes structural interpretations of the magnetite surface developed by Vayssières et al. (1998), predicts a number of possible surface species, charges and structural configurations, depending on the crystal planes chosen to define the surface of each face. For the following calculations, crystal planes which expose oxygens bound to iron atoms in both tetrahedral and octahedral coordination were selected (Jolivet and Hernandez, 1999). Five independent surface protonation reactions are predicted to have $\log K_{Hy}$ values in the accessible pH range (i.e., 0–14), and thus the ability to protonate and deprotonate in natural aqueous solutions:

$$-FeOH^{-0.58} + H_s^+ \Leftrightarrow -FeOH_2^{0+0.42} \qquad K_{H1} \quad (16)$$

$$-FeOH^{-0.24} + H_s^+ \Leftrightarrow -FeOH_2^{0+0.76} \qquad K_{H2} \quad (17)$$

$$-Fe_3O^{-0.42} + H_s^+ \Leftrightarrow -FeO_3H^{0+0.58} \qquad K_{H3} \quad (18)$$

$$-Fe_3O^{-0.75} + H_s^+ \Leftrightarrow -FeO_3H^{0+0.25} \qquad K_{H4} \quad (19)$$

$$-Fe_2O^{-0.84} + H_s^+ \Leftrightarrow -FeO_2H^{0+0.16} \qquad K_{H5} \quad (20)$$

The protonation constants (formulated as in Eq. 12) for these reactions at 25°C calculated from the structural analysis of Jolivet and Hernandez (1999), using the revised MUSIC model of Hiemstra et al. (1996), are given in Table 3, along with the percentages of each site type on each face, the total site density for each face, and the calculated $pH_{ppzc}$ of each face. The $s_{Me-O}$, $m$ and $n$ parameter values for use in Eq. (15) are also given in Table 3. As can be seen in Table 3, each face has a distinctly different $pH_{ppzc}$. SEM examination of the solid phase used in this study (e.g., Fig. 2) indicates that the 110 and 100 faces are predominantly developed, with the 111 face of more minor importance. For application of the MUSIC model, we assumed that a face distribution of 57% (110), 23% (100), and 20% (111) was reasonable. The distribution of faces, which is qualitatively consistent with the SEM observations, was manipulated in order to give a 25°C calculated net $pH_{ppzc}$ (6.87) in reasonable agreement with the results of this study, 7.00 (Eq. 13), the value 6.9 from the data of Blesa et al. (1984), and the value of 7.1 predicted by Sverjensky and Sahai (1996).

The constant $A^{25°C}$ in Eq. (15) was determined by Hiemstra et al. (1996) to be 19.80. Machesky et al. (2000) have developed a similar correlation, using a number of metal ion hydrolysis constants derived

Table 3
MUSIC model surface speciation and proton binding constants (Eqs. 16–20) at 25°C predicted for the magnetite surface, percentage of each site type on each face, total site densities, and resulting $pH_{ppzc}$ values computed for each face using the revised MUSIC model (Hiemstra et al., 1996) and the crystal structural analysis of Jolivet and Hernandez (1999)

| | $s_{Me-O}$ (Eq. 15) | $m$, $n$ (Eq. 15) | $\log K_{Hy}$ | Percent[a] | Density[b] | $pH^{c}_{ppzc}$ |
|---|---|---|---|---|---|---|
| *111 Face with oxygen atoms coordinated to octahedral $Fe^{2.5+}$ and tetrahedral $Fe^{3+}$* | | | | | | |
| $-Fe_2O^{-0.84} + H_s^+ \Leftrightarrow -FeO_2H^{0+0.16}$ $K_{H5}$ | 0.417, 0.741 | 0, 2 | 9.594 | 75.0 | $2.46 \times 10^{-5}$ | 8.52 |
| $-FeOH^{-0.24} + H_s^+ \Leftrightarrow -FeOH_2^{0+0.76}$ $K_{H2}$ | 0.741 | 1, 1 | 5.625 | 25.0 | | |
| *100 Face with oxygen atoms coordinated to octahedral $Fe^{2.5+}$ and tetrahedral $Fe^{3+}$* | | | | | | |
| $-Fe_3O^{-0.75} + H_s^+ \Leftrightarrow -FeO_3H^{0+0.25}$ $K_{H4}$ | 0.417, 0.417, 0.417 | 0, 1 | 11.907 | 33.3 | | |
| $-Fe_3O^{-0.42} + H_s^+ \Leftrightarrow -FeO_3H^{0+0.58}$ $K_{H3}$ | 0.417, 0.417, 0.741 | 0, 1 | 4.883 | 33.3 | $2.85 \times 10^{-5}$ | 11.32 |
| $-FeOH^{-0.58} + H_s^+ \Leftrightarrow -FeOH_2^{0+0.42}$ $K_{H1}$ | 0.417 | 1, 1 | 12.649 | 33.3 | | |
| *110 Face with oxygen atoms coordinated to octahedral $Fe^{2.5+}$ and tetrahedral $Fe^{3+}$* | | | | | | |
| $-Fe_3O^{-0.42} + H_s^+ \Leftrightarrow -FeO_3H^{0+0.58}$ $K_{H3}$ | 0.417, 0.417, 0.741 | 0, 1 | 4.883 | 40.0 | | |
| $-FeOH^{-0.58} + H_s^+ \Leftrightarrow -FeOH_2^{0+0.42}$ $K_{H1}$ | 0.417 | 1, 1 | 12.649 | 40.0 | $4.54 \times 10^{-5}$ | 6.30 |
| $-FeOH^{-0.24} + H_s^+ \Leftrightarrow -FeOH_2^{0+0.76}$ $K_{H2}$ | 0.741 | 1, 1 | 5.625 | 20.0 | | |

[a] Percentage of each site type on each face.
[b] Total site density on each face, in $mol/m^2$.
[c] Net $pH_{ppzc}$ for each face computed from a site–density weighted average of the $K_{Hy}$ values and Eq. (21).

from the recent experimental literature and the revised HKF predictions of aqueous metal hydrolysis reactions of Shock et al. (1997), obtaining a somewhat larger $A'^{25°C}$ parameter of 21.70, which was used to calculate the protonation constants in Table 3. The same regression analysis was extended to 300°C, with revised $A'$ parameters listed as a function of temperature in Table 4. Machesky et al. (2000) propose that a useful approximation for calculating the temperature dependence of $\log K_{Hy}$ values generated from the MUSIC model can be made by assuming that these revised A′ values represent the only temperature dependent term in Eq. (15). Machesky et al. (2000) further demonstrate that $pH_{ppzc}$ values for rutile calculated using this assumption lie within 0.06 log units of the experimentally derived $pH_{ppzc}$ values from 25°C to 250°C.

Using this approximation, together with Eq. (15) and the relation

$$pH_{ppzc,y} = \log K_{Hy} + \log\{|z|/(1-|z|)\} \qquad (21)$$

where $pH_{ppzc,y}$ is the pH at which the charge-weighted concentrations of positively and negatively charged surface species associated with site $y$ are equal, and $z$ is the fractional negative charge on the deprotonated surface site (e.g., $-0.58$ for $K_{H1}$ in reaction 16). The overall $pH_{ppzc}$ for the magnetite used in this study, can be calculated by averaging the $pH_{ppzc,y}$ values for each site, and incorporating the

Table 4
Revised A′ parameters derived by Machesky et al. (2000) for use in extrapolating the revised MUSIC model proton binding constants (Hiemstra et al., 1996) to elevated temperatures, along with $K_{Hy}$ values corresponding to the protonation reactions in Table 3 and Eqs. 16–20, and the overall $pH_{ppzc}$ for magnetite

| $T$ (°C) | $A'$ | log $K_{H1}$ | log $K_{H2}$ | log $K_{H3}$ | log $K_{H4}$ | log $K_{H5}$ | net $pH^{a}_{ppzc}$ |
|---|---|---|---|---|---|---|---|
| 0 | 23.254 | 13.555 | 6.027 | 5.232 | 12.759 | 10.280 | 7.262 |
| 25 | 21.700 | 12.649 | 5.625 | 4.882 | 11.907 | 9.549 | 6.870 |
| 50 | 20.490 | 11.943 | 5.311 | 4.610 | 11.243 | 9.058 | 6.564 |
| 100 | 18.713 | 10.908 | 4.850 | 4.210 | 10.268 | 8.273 | 6.110 |
| 125 | 18.103 | 10.552 | 4.692 | 4.073 | 9.933 | 8.003 | 5.952 |
| 150 | 17.647 | 10.287 | 4.574 | 3.971 | 9.683 | 7.802 | 5.833 |
| 175 | 17.242 | 10.050 | 4.469 | 3.879 | 9.461 | 7.623 | 5.726 |
| 200 | 16.917 | 9.861 | 4.385 | 3.806 | 9.282 | 7.479 | 5.640 |
| 225 | 16.658 | 9.710 | 4.318 | 3.748 | 9.140 | 7.365 | 5.571 |
| 250 | 16.452 | 9.590 | 4.264 | 3.702 | 9.027 | 7.274 | 5.515 |
| 275 | 16.287 | 9.493 | 4.221 | 3.664 | 8.936 | 7.200 | 5.471 |
| 300 | 16.143 | 9.410 | 4.184 | 3.632 | 8.858 | 7.137 | 5.432 |

[a] Overall $pH_{ppzc}$ for an entire magnetite particle exhibiting the following distribution of faces (110, 57%), (100, 23%) and (111, 20%).

density of each site on each face, and the assumed overall distribution of faces, as shown in Fig. 8 and listed in Table 4. As can be seen, these extended MUSIC model estimates lie within the assigned uncertainty of the $pH_{infl}$ values determined from our 0.03 molal isotherms at all temperatures investigated.

Note that according to the MUSIC model, at the overall $pH_{ppzc}$, some faces will still carry positive or negative net proton-induced charge. If correct, this has interesting implications for the face-specific incorporation of trace elements onto mineral surfaces via sorbtive processes, as well as the face-specific growth and dissolution of the mineral itself and the orientation of colloidal particles of such a mineral deposited onto charged surfaces during transport through porous media.

### 5.2. Surface charge modeling

Surface complexation modeling of proton adsorption data combines chemical descriptions of surface hydroxyl (S–OH) group behavior with coulombic or electrostatic corrections based on an assumed EDL structure. Several models have been commonly used to describe proton adsorption by oxide surfaces near room temperature. Proton adsorption isotherms for rutile between 25°C and 250°C could be rationalized using either a one-p$K$, three-layer EDL model with the $pH_{ppzc}$ values equated to the observed $pH_{cip}$ values, or the temperature-extrapolated MUSIC model estimates for the $pH_{ppzc}$, coupled with a basic Stern layer model and variable capacitance and ion binding constants (Machesky et al., 1998, 2000). Modeling of the observed magnetite sorption isotherms using the MUSIC model $K_{Hy}$ values listed in Table 4 is currently underway, and will be the subject of a subsequent communication. Here, we provide an analysis of the magnetite surface charge data in terms of the one-p$K$ model approach discussed above.

Examination of Fig. 4 demonstrates that the $pH_{infl}$ as well as the $pH_{cip}$ values at most temperatures studied lie at $\mu mol\ H^+/m^2$ values well above the zero proton condition. This was also observed in our initial studies of rutile (Machesky et al., 1994), with ''offsets'' from the zero proton condition of similar magnitude and direction. Subsequent experiments with hydrothermally pretreated rutile essentially eliminated this artifact (Machesky et al., 1998) and it was tentatively attributed to a protolytic impurity in the solid phase, perhaps residual HCl sequestered in the solid during the synthesis process. In order to avoid oxidation of the magnetite produced from the Ni/NiO method described above, we chose not to hydrothermally pretreat the solid prior to the titration experiments reported in this study. In order to model the surface charge of magnetite from the experimental proton sorption isotherms, an ''offset'' correction was applied to the sorption isotherms, which is essentially a correction factor for the presence of a protolytic impurity in the solid that is not accounted for in the background (solution blank) correction, in a similar manner to the much smaller offset corrections applied to the improved rutile titration results (Machesky et al., 1998). Initial modeling efforts in which the offset correction was included as an adjustable fit parameter indicated that the values closely approach the observed offset at the $pH_{cip}$. Furthermore, residual proton-induced negative surface charge is expected at the $pH_{ppzc}$ in the presence of strong cation binding (Stumm, 1992). A modified form of Eq. (9) was thus used to calculate the net proton-induced surface charge density:

$$\sigma_H = (\text{''solution excess''}\ \mu mols\ H^+/m^2 - \text{''offset correction''}) * (-F) \quad (22)$$

Offset correction values (Table 5) for use in Eq. (22) were arbitrarily assigned as the observed background-corrected $\mu mol\ H^+/m^2$ value at the observed $pH_{cip}$ at each temperature, and the offset-corrected surface charge curves are plotted in Fig. 10. In essence, these offset corrections equate the observed $pH_{cip}$ values with $\sigma_H = 0$.

#### 5.2.1. One-pK, two layer model equations

The EDL configuration used in this study is illustrated in Fig. 11. The EDL structure includes protonation at the mineral surface, defined by $K_H$, specific cation and anion binding at a Stern layer in solution, defined by $K_{M1}$ and $K_{A1}$, and a diffuse layer of cations and anions defined by Guoy–Chapman theory. The zeta potential ($\zeta$) is taken to equal the diffuse layer potential ($\Psi_D$) at the outermost

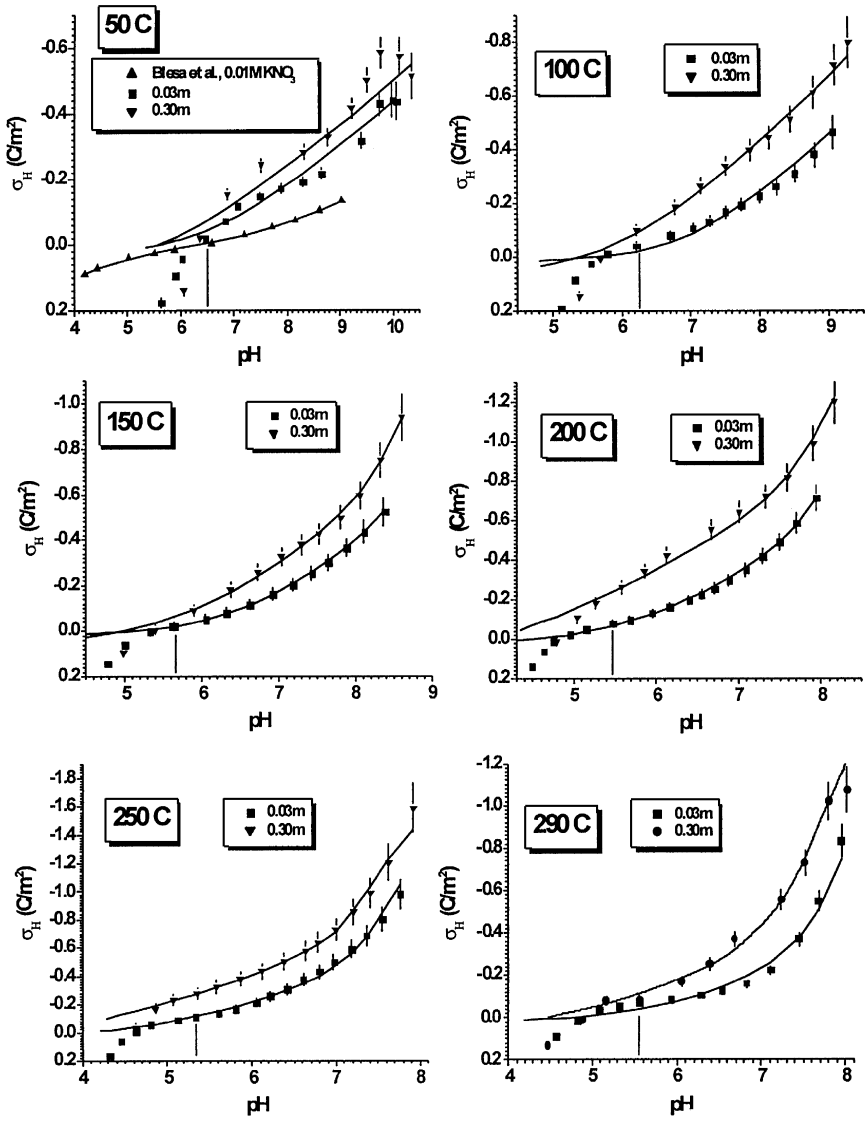


Fig. 10. Proton-induced surface charge density, $\sigma_H$ in $C/m^2$, computed from the results of this study using Eq. (22) and the isotherm data in the Appendix, with offset corrections listed in Table 5. The symbols represent the individual titration points with associated error estimates (Appendix) and the smooth curves were generated from the one-p$K$, two layer model discussed in the text. Also shown in (a) are results reported by Blesa et al. (1984) in 0.01M $KNO_3$ at 50°C, fitted using the same model (Table 5).

Stern plane, which is not equal to the potential at the anion layer ($\Psi_A$), as in the triple-layer-model of Sverjensky and Sahai (1996). There is also provision in the model for cation binding directly at the mineral surface, defined by $K_{M2}$, such that these ions experience the surface potential, $\Psi_0$.

The relevant surface protonation constant can be given as,

$$K_H = \left[FeOH_2^{+0.5}\right]/\left(\left[FeOH^{-0.5}\right]\{H^+\}_b \times \exp(-z_H F\Psi_o/RT)\right) \quad (23)$$

analogous to reaction (12) for rutile, with symbols

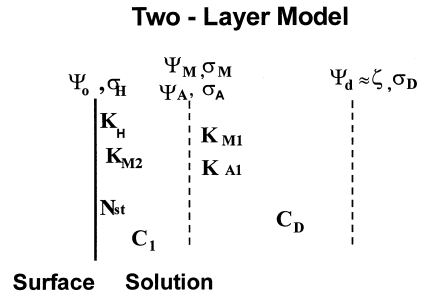


Fig. 11. Schematic representation of the one-p$K$, two-layer model.

defined in the same way, and values of $\log K_H$ assumed equal to the $pH_{infl}$ values (Table 2).

Cation binding constants are given as,

$$K_{M1} = \left[FeOH^{-0.5}{-}M^{+}\right] / \left(\left[FeOH^{-0.5}\right]\left[M^{+}\right]_b \times (\gamma \pm_{NaTr}) \exp(-z_M F \Psi_M / RT)\right) \quad (24)$$

$$K_{M2} = \left[FeOH^{-0.5}{-}M_s^{+}\right] / \left(\left[FeOH^{-0.5}\right]\left[M^{+}\right]_b \times (\gamma \pm_{NaTr}) \exp(-z_M F \Psi_o / RT)\right) \quad (25)$$

where $[M^+]_b$ = bulk cation concentration (molal), $\gamma \pm_{NaTr}$ = mean molal stoichiometric activity coefficient of NaTr at a given ionic strength and temperature (assumed equal to the activity coefficient of NaCl at the same temperature and ionic strength from Archer, 1992), $z_M$ is the cation charge, and $\Psi_M$ = potential at the edge of the Stern plane. Similarly, an anion binding constant is defined as,

$$K_{A1} = \left[FeOH_2^{+0.50}{-}A\right] / \left(\left[FeOH_2^{+0.50}\right]\left[A^{-}\right]_b \times (\gamma \pm_{NaTr}) \exp(-z_A F \Psi_A / RT)\right) \quad (26)$$

where, $[A^-]_b$ = bulk anion concentration (molal), $z_A$ is the anion charge, and $\Psi_A$ = potential at the plane of anion adsorption (equal to $\Psi_M$ using the Basic Stern Model). Finally, the total surface site concentration is,

$$N_{st} = \left[FeOH_2^{+0.5}\right] + \left[FeOH^{-0.5}\right] + \left[FeOH^{-0.5}{-}M^{+}\right] + \left[FeOH^{-0.5}{-}M_s^{+}\right] + \left[FeOH_2^{+0.5}{-}A^{-}\right] \quad (27)$$

where $N_{st}$ is the total site density (mol/m$^2$).

The capacitance values for the two layers ($C_1$ and $C_D$) were the parameters used to determine the potentials associated with these layers. The capacitance value of the outer most layer ($C_D$) was fixed, based on the so-called double-layer thickness at each temperature and ionic strength. This capacitance was included in our EDL model to provide a means to simulate and predict zeta potentials for magnetite. Zeta potential values for magnetite reported by Regazzoni et al. (1983) are reasonably well simulated by fixing the $C_D$ value using the double layer

Table 5
One-p$K$ model parameters for magnetite proton surface charge curves (Fig. 10)

| $T$ (°C), $I$ | pH range | Offset (F) | $C_1$ | SD | $C_D$ (F) | $K_{M1}$ | SD | $K_{A1}$ | SD | $K_{M2}$ | SD | MSC |
|---|---|---|---|---|---|---|---|---|---|---|---|---|
| 50, 0.03 | 10.1–6.8 | −0.038 | 2.500(F) | | 0.363 | 2.047 | 0.361 | | | | | 2.55 |
| 50, 0.30 | 10.4–6.4 | −0.038 | 2.500(F) | | 1.152 | 0.765 | 0.256 | | | | | 2.51 |
| 50, 0.01[a] | 4.2–9.0 | 0.0 | 1.450 | 0.10 | 0.209 | 0.624 | 0.110 | 0.272 | 0.041 | | | 5.80 |
| 100, 0.03 | 9.1–5.8 | 1.688 | 4.494(F) | | 0.310 | 0.584 | 0.058 | | | | | 3.38 |
| 100, 0.30 | 9.3–5.7 | 1.688 | 4.494(F) | | 0.983 | 0.552 | 0.059 | | | | | 4.33 |
| 150, 0.03 | 8.4–5.3 | 2.489 | 3.820(F) | | 0.268 | 0.630 | 0.301 | | | 0.01790 | 0.0028 | 5.84 |
| 150, 0.30 | 8.6–5.4 | 2.489 | 3.820(F) | | 0.849 | 0.346 | 0.037 | | | 0.00638 | 0.0008 | 4.62 |
| 200, 0.03 | 7.9–5.2 | 1.896 | 3.240(F) | | 0.231 | 2.761 | 0.161 | | | 0.09057 | 0.0075 | 4.95 |
| 200, 0.30 | 8.2–5.0 | 1.896 | 3.240(F) | | 0.738 | 6.071 | 0.909 | | | 0.02823 | 0.0050 | 3.75 |
| 250, 0.03 | 7.8–4.8 | 1.219 | 2.350(F) | | 0.201 | 8.659 | 0.756 | | | 0.24930 | 0.0146 | 4.64 |
| 250, 0.30 | 7.9–4.9 | 1.219 | 2.350(F) | | 0.643 | 17.286 | 1.476 | | | 0.08503 | 0.0047 | 4.95 |
| 290, 0.03 | 8.0–5.1 | 0.618[b] | 1.850(F) | | 0.179 | 1.333 | 0.397 | | | 0.12839 | 0.0218 | 2.41 |
| 290, 0.30 | 8.0–5.2 | 1.242[b] | 1.850(F) | | 0.575 | 1.978 | 0.525 | | | 0.07046 | 0.0079 | 3.57 |

[a] Data of Blesa et al. (1984) in $KNO_3$.
[b] Offset correction adjusted to give zero μmol at the $pH_{cip}$ from Table 2.

thickness. This has also been noted by Hiemstra et al. (1999) in their studies of Al oxides, although this assumption resulted in either too high or too low zeta potential estimates in some of their simulations.

The EDL potential values can be expressed as,

$$\Psi_0 = (\sigma_H/C_1) + (-\sigma_D/C_D) + \Psi_D \quad (28)$$

$$\Psi_D = \zeta = (2RT/F)\operatorname{arcsinh}\left(-\sigma_d/(8RT\varepsilon_0\varepsilon_b I\rho_s)^{1/2}\right) \quad (29)$$

$$\Psi_A = \Psi_M = \Psi_0 - (\sigma_H/C_1) \quad (30)$$

where $\sigma_H$ is the proton-induced surface charge,

$$\sigma_H = F\{[FeOH_2^{+0.5}](z+z_H) + [FeOH_2^{+0.5}\text{–}A^-](z+z_H) + [FeOH^{-0.5}](z) + [FeOH^{-0.5}\text{–}M^+](z) + [FeOH^{-0.5}\text{–}M_s^+](z)\} \quad (31)$$

$\sigma_D$ is the uncompensated or diffuse layer charge,

$$\sigma_D = -F\{[FeOH_2^{+0.5}](z+z_H) + [FeOH_2^{+0.5}\text{–}A^-] \times (z+z_H+z_A) + [FeOH^{-0.5}](z) + [FeOH^{-0.5}\text{–}M^+](z+z_M) + [FeOH^{-0.5}\text{–}M_s^+](z+z_M)\} \quad (32)$$

$C_D$ is the diffuse layer capacitance from Guoy–Chapman theory

$$C_D = \varepsilon_0\varepsilon_b 2.32\times10^9(\varepsilon_{298}2I\rho_s 298/(\varepsilon_b T))^{1/2} \quad (33)$$

where $z = -0.50$, $\varepsilon_0$ = permittivity of vacuum = $8.854\times10^{-12}$, $\varepsilon_b$ = bulk dielectric constant of water at a given temperature and ionic strength, $I$ = stoichiometric molal ionic strength, and $\rho_s$ = solution density which was taken from the properties of NaCl solutions at the same temperature and ionic strength (Archer, 1992). The solution density term is necessary since the Guoy–Chapman theory, which is used to calculate $\Psi_D$ above, is typically formulated in terms of molar concentration units. The term within parentheses in Eq. (33) is commonly referred to as $\kappa$ ($m^{-1}$ units), the inverse of which is the so-called double-layer thickness. Finally, electroneutrality requires that,

$$\sigma_H + \sigma_M + \sigma_A + \sigma_D = 0 \quad (34)$$

where, $\sigma_A$ is the anion charge at the Stern plane,

$$\sigma_A = F(z_A)\{[FeOH_2^{+0.5}\text{–}A^-]\} \quad (35)$$

and $\sigma_M$ is the cation charge at the Stern plane,

$$\sigma_M = F(z_M)\{[FeOH^{-0.5}\text{–}M^+]\} \quad (36)$$

*5.2.2. Modeling results*

Model parameters which remained fixed during the fitting exercise were, the offset values, $C_D$ (the diffuse layer capacitance), the surface protonation constant ($K_H$), and the anion binding constant ($K_{A1}$) which was fixed at a very low value ($10^{-8}$) to reflect the fact that the triflate anion is not expected to interact significantly with the negatively charged magnetite surface (Table 5). The surface site density ($N_{st}$) could also be fixed at $3.62\times10^{-5}$ mol/$m^2$, and this is close to the weighted average value for the 100, 110 and 111 faces given by Jolivet and Hernandez (1999). The innermost capacitance value ($C_1$) was also fixed during the final modeling simulations at the maximum value expected based on the radius of $Na^+$ at temperatures of 100°C and above (Machesky et al., 1998). These values decrease with increasing temperature in proportion to the decreasing dielectric constant of water. The second cation binding constant, $K_{M2}$, was set to a very low value ($10^{-8}$) at 100°C and below. The only fitting parameter that was always allowed to vary was $K_{M1}$.

Relative weights were assigned to each data point computed from Eq. (22), using the estimated uncertainty in the computed excess or deficit of $H^+$ in solution (Appendix),

$$W_i = (\text{error}_{max})^2/(\text{error}_i)^2 \quad (37)$$

where, $\text{error}_{max}$ is the maximum error value for a particular titration, and $\text{error}_i$ is the error associated with a particular titration point. Commercially available software (SCIENTIST, Micromath, Orem, UT) was used to fit the weighted surface charge ($\sigma_H$) values to the two-layer model with pH as the independent variable.

Table 5 summarizes the titration experiments modeled, along with associated fixed ($F$) and variable fitting parameters. Also included are standard deviations (SD) for the variable parameters (a blank SD cell means a fixed parameter value), the pH

range over which the fitting was conducted, and the model selection criterion (MSC), which is a measure of the goodness-of fit (larger is better). The entire pH range of a particular titration was not modeled, because the sharp downturn in the sorption isotherms below the $pH_{cip}$, attributed to magnetite dissolution, is not a true representation of surface charging processes. Model curves are presented as the solid lines in Fig. 10.

The fit of the two-layer model to the titration curves is generally good over the pH range modeled. Note that the model predicts that the surface is negatively charged at the assumed $pH_{ppzc} = \log K_H$, indicated by the vertical lines in Fig. 10. This is indicative of strong specific cation binding. The conventional approach to dealing with background electrolyte binding within the context of the one-p$K$ model is to consider single binding constants for the electrolyte cation and anion. However, our corrected proton charge curves are fairly asymmetric above 100°C. That is, above the $pH_{cip}$, negative proton charge development at first increases rather gradually and then much more steeply with increasing pH. This is indicative of progressively more efficient screening of negative proton charge by $Na^+$ with increasing pH. The steepness and asymmetry of apparent negative charge development might also be related to a thick hydrated surface layer, as discussed in Section 3. If the BET surface area is significantly lower than the ''reactive'' surface area, in terms of sorption of ions, then the apparent steepness of the isotherms may be an artifact, since the surface area appears in the denominator of Eq. (22). Alternatively, a hydrated surface layer may allow penetration of solution ions into the surface of the solid. At this time, we have no direct evidence to support either of these hypotheses.

Preliminary modeling efforts demonstrated that it was not possible to fit satisfactorily this steep increase in negative proton-induced charge development with a single binding constant and distance of charge separation for $Na^+$. There are various modeling alternatives that might have been utilized to adequately simulate this portion of the charging curves. We have chosen to include a second cation binding constant, $K_{M2}$, which allows a portion of the $Na^+$ to experience the surface potential rather than the Stern plan potential (Eq. 25). A similar approach was taken by Hiemstra et al. (1999) to better model (with a one-p$K$ approach) the charge asymmetry they observed for $\gamma$-$Al_2O_3$ surface titration data. In any case, a finite $K_{M2}$ value is only required at 150°C and above, which reflects more efficient screening of negative surface charge development with increasing temperature as was observed for rutile (Machesky et al, 1998).

It should be kept in mind that the model description of negative surface charge neutralization is primarily reflected in the combined effects of the $C_1$, $K_{M1}$ and $K_{M2}$ parameter values. These variables are highly covariant, and it is difficult to generalize the effect of individual parameters, particularly in terms of systematic trends of the parameter values with temperature and ionic strength. The mass action equilibria permit $Na^+$ to bind with the negatively charged surface, thus allowing more proton-induced negative surface charge density to develop. However, in a somewhat similar way, increasing the $C_1$ value brings the plane of counterion charge closer to the surface plane, with the result that neutralization of surface charge development is more efficient. This permits more surface charge to develop at a given pH value. Moreover, over a certain range of values, a decrease in $C_1$ can be compensated for by an increase in the counterion binding constants. In other words, more binding at a greater distance from the surface is not easily distinguished from less binding closer to the surface. Thus, it is not possible to unequivocally distinguish between the intrinsic (e.g., $K_{M1}$) and electrostatic (e.g., $C_1$) components of counterion binding. Consequently, it is the combination of these parameters that is typically most useful in rationalizing surface charge development.

As can be best seen in Fig. 5, negative surface charge increases from 50°C to 250°C, but then decreases somewhat between 250°C and 290°C. This is reflected in lower best-fit $K_{M1}$ and $K_{M2}$ values at the higher temperature. Possible reasons for this decrease include reconstitution of the magnetite surface during the titration at this extreme temperature, and experimental artifacts associated with the large solution blank correction. Furthermore, it was not possible to satisfactorily fit our 0.03 and 0.30 molal data with the same $K_{M1}$ and $K_{M2}$ values at a given temperature, although the best fit values at the two ionic strengths at each temperature generally vary by

less than a factor two for $K_{M1}$ and four to five for $K_{M2}$.

Fig. 10a compares our 50°C titration curves with comparable data from Blesa et al. (1984) in 0.01 M $KNO_3$ at 50°C. Estimated $pH_{ppzc}$ values from the two studies are virtually identical at this temperature (6.50 and 6.45), but our surface charge curves are considerably steeper, as reflected in the larger best-fit $C_1$ values for our titration curves (Table 5). Part of this difference is due to the different background electrolytes used. The larger $K^+$ ion should interact less specifically with the magnetite surface than $Na^+$. Also, the data from Blesa et al. (1984) were not obtained at the same ionic strengths as our titrations, and only their data in 0.01 M data are shown in Fig. 10a. Note that our surface charge curves are considerably steeper below about pH 6.4 because of significant magnetite dissolution. The results of Blesa et al. (1984) do not seem to be significantly influenced by dissolution, probably because the titrations were conducted much more rapidly. Corresponding parameter values used to fit the data of Blesa et al. (1984) at 50°C in 0.01 M $KNO_3$ are listed in Table 5. A significant $K_{A1}$ value was needed to fit the data of Blesa et al. (1984), because of the observed positive surface charge data below the $pH_{ppzc}$.

These preliminary modeling efforts are certainly not as well constrained as those obtained for rutile over a similar range of temperature and ionic strength (Machesky et al., 1998, 1999). This reflects the greater reactivity of the magnetite surface with respect to $Na^+$ interaction at higher pH, and the dissolution of magnetite at lower pH values. These effects, combined with the large solution blank corrections, result in net proton sorption isotherms from which it is difficult to unambiguously identify where $\sigma_H = 0$. However, the model results depend on relatively few ($C_1$, $K_{M1}$, and $K_{M2}$) fitting parameters. Moreover, we anticipate that additional studies of magnetite and other metal oxides over a broad range of temperature and ionic strength, coupled with other methods to probe these surfaces, will lead to more highly constrained and realistic models in the future.

### *5.3. Preliminary results with higher surface area material*

As discussed in Section 3 above, a new batch of magnetite has been synthesized in our laboratories which has nearly twice the surface area (1.72 $m^2/g$) as the 0.92 $m^2/g$ material used for the bulk of this investigation. Results of preliminary surface titrations with this new material are shown in Fig. 12 in

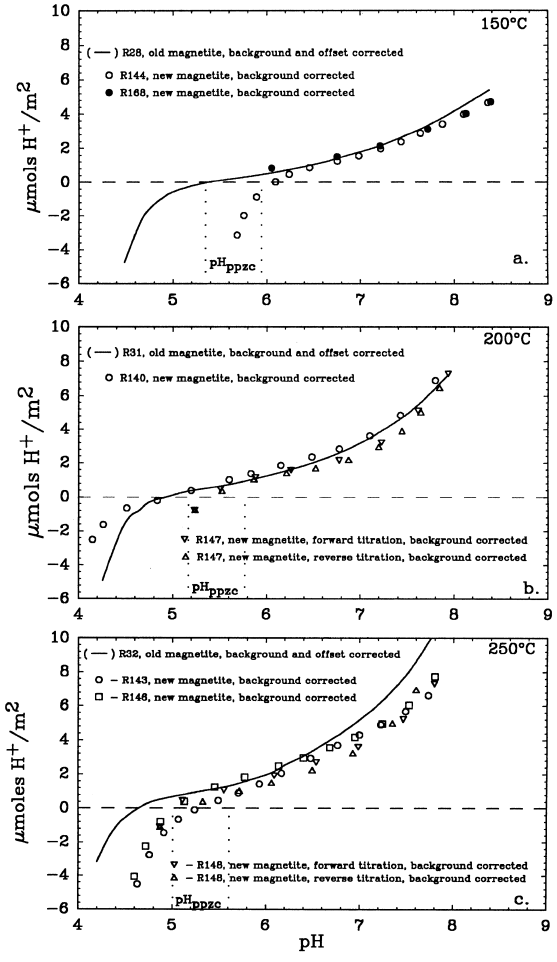


Fig. 12. Proton sorption isotherms in 0.03 molal NaTr obtained with a higher surface area (1.72 $m^2/g$) treated Alfa lot#22387 magnetite (symbols representing individual titration points) at (a) 150°C, (b) 200°C and (c) 250°C. The solid curves represent the background and offset corrected sorption isotherms obtained with the lower surface area magnetite (0.92 $m^2/g$) used for the bulk of the studies. Inverse triangles in (b) and (c) represent ''forward'' titrations conducted in the normal sense relative to all other titration data discussed in the text, and the upright triangles represent ''reverse'' titrations in the same experiment, using a second pump loaded with base titrant. Dotted lines represent the uncertainty range of the estimated $pH_{ppzc}$ obtained from the 0.92 $m^2/g$ magnetite.

0.03 molal NaTriflate at 150, 200 and 250°C, with the same background (solution blank) correction applied as was used to correct the data from the lower surface area material. However, the influence of this background correction on the data from the new solid is reduced proportionally to the ratio of surface areas. The SHECC apparatus used for these new studies was fitted with a second positive displacement pump, enabling both acidic and basic titrants to be delivered to the test solution during an individual experiment. As discussed above, the bulk of our experiments were conducted by first equilibrating the magnetite with a basic test solution, then titrating with acid, referred to as ''forward'' titrations. Runs 147 and 148 at 200°C and 250°C with the new magnetite were reversed by addition of a basic titrant after the normal sorption isotherm data were collected. As can be seen in Fig. 12b and c, there is almost no hysteresis in the reverse titrations, although the forward titrations were truncated at a relatively high pH in order to avoid extensive dissolution of magnetite.

Also shown as solid curves in Fig. 12 are the equivalent isotherms obtained with the lower surface area (''old'') magnetite at the same temperature and ionic strength (Appendix), but corrected for both background and the offset values listed in Table 5. The most significant observations from these new results are that the isotherms obtained with the new solid are nearly coincident with those obtained from the old solid, and the slopes of the isotherms are very similar at 150°C and 200°C and only moderately shallower at 250°C, compared with the equivalent isotherms obtained with the lower surface area solid. Furthermore, no offset correction was applied to the new results, suggesting that if a protolytic impurity in the lower surface area solid was the cause of these offsets, it is not present in significant quantities in the new solid. This could possibly be a result of the use of a different lot of Alfa Puratronic Fe(II)Fe(III) oxide (see Section 3), or could be related to the fact that the new solid was first ground to a considerably finer grain size before the $Ni/NiO/H_2O$ pretreatment. This may have exposed ''cleaner'' material in the interiors of magnetite grains, which then may have overcoated the ''contaminated'' surface of the commercial material during recrystallization in the pretreatment step.

The isotherms obtained with the new material exhibit the sharp downturn associated with significant dissolution of the solid at higher pHs than the ''old'' magnetite, with the exception of run 140 at 200°C. This suggests that the higher surface area magnetite more rapidly dissolves, and the lack of reproducibility of this dissolution effect supports the argument made above that it is a kinetically controlled phenomenon strongly influenced by the timing of individual experiments. Additional surface titrations will be conducted in our laboratories with this new material. However, the increased dissolution effect may limit the useful data range to the higher pHs.

These preliminary results with a different batch of magnetite, possessing nearly twice the surface area and apparently lower levels of some protolytic impurity, compared with the ''old'' magnetite, strongly support the conclusions drawn from the bulk of the experiments. The background correction appears to be at least qualitatively reliable, and the measured excess $H^+$ in solution quantitatively varies in proportion to the surface area of solid exposed to the solution. Finally, the offset effect observed with the lower surface area material does indeed appear to be a property of the individual batch of solid used, or some aspect of the solid handling procedure, as was also observed for rutile (Machesky et al., 1994, 1998). The reversibility without hysteresis of the isotherms obtained with the new material also demonstrates that the offset effect observed with the old solid is not simply an artifact of the pH of the starting point of the titration. These new titration results also support the modeling results and $pH_{ppzc}$ estimates, in that the isotherms with the new magnetite are nearly as steep at high pH as the previous results, and the new isotherms approach the zero $\mu mol\ H^+/m^2$ condition near the predicted $pH_{ppzc}$ values obtained from the old solid ($pH_{infl}$) as well as the MUSIC model predictions.

## 6. Summary and conclusions

Commercially available, as well as conventionally synthesized, magnetite was invariably found to contain 10–30% oxidized iron oxide, in the form of $\alpha$- or $\gamma$-$Fe_2O_3$, which appeared to reduce the surface

charge density significantly at a given pH, temperature and ionic strength. This problem was overcome by developing a treatment method which involved reaction of commercial magnetite under the hydrogen fugacity imposed by the $Ni/NiO/H_2O$ buffer for a period of 5 days to 2 weeks at 500°C. The resulting material proved to be nearly pure, well-crystallized, stoichiometric magnetite, with well developed 110, 100 and 111 faces.

Direct potentiometric pH titrations were successfully performed with this magnetite in 0.03 and 0.30 molal NaTr solutions from 50°C to 290°C and at pHs spanning mildly acidic to strongly basic conditions, using methodologies similar to our recent studies of rutile surface charge (Machesky et al., 1994, 1998). NaTriflate was used as the supporting electrolyte in these studies, rather than NaCl (used in our rutile studies) in order to minimize dissolution of the solid phase by the formation of soluble iron–chloride complexes. Despite this precaution, significant dissolution of the magnetite occurred in the low-pH range of each titration. Sampling of equivalent titrations indicated that the solutions remain undersaturated by many orders of magnitude with respect to magnetite alone at hydrogen partial pressures of 10–20 bars, but approach the concentration levels predicted for a metastable reaction involving removal of ferrous iron from the magnetite surface and conversion to hematite, under redox disequilibrium conditions. Because the iron level in solution was shown to be kinetically controlled and dependent on the exact timing of sample extraction, it proved impractical to make solubility corrections to the observed sorption isotherms. However, the absolute magnitude of these corrections is shown to be insignificant in the pH range near and above the zero point of charge of the surface at all conditions.

The background-corrected magnetite surface sorption isotherms in 0.03 and 0.30 molal NaTriflate at 50–290°C were shown to intersect at common points ($pH_{cip}$), which are interpreted in this study to be somewhat lower than the actual $pH_{ppzc}$ values due to significant specific binding of $Na^+$ with the negatively charged magnetite surface. The $pH_{ppzc}$ of magnetite was estimated from inflection points ($pH_{infl}$) in the 0.03 molal surface sorption isotherms, which lie above the $pH_{cip}$ values, as also predicted if significant cation binding occurs. These $pH_{ppzc}$ values are shown to be in good agreement with equivalent values predicted independently from the magnetite surface structure, using the MUSIC or multisite complexation model of Hiemstra et al. (1996), together with the magnetite surface species calculations of Jolivet and Hernandez (1999). The MUSIC model $pH_{ppzc}$ values were estimated at elevated temperatures by an analysis of the temperature dependence of a large number of homogeneous aqueous protonation reactions (Machesky et al., 2000). The $pH_{ppzc}$ values derived in this study are in fairly good agreement with the theoretical estimate of Sverjensky and Sahai (1996) at 25°C and the experimental measurements of Blesa et al. (1984) to 80°C. An interesting implication of the MUSIC model approach is that some magnetite crystal faces will retain a net positive or negative proton-induced surface charge at the overall $pH_{ppzc}$. This may influence the growth and dissolution rates of certain faces, and even individual sites within a face. Incorporation of trace elements from solution is also likely to be influenced by this face-specific charging behavior.

The surface protonation isotherms for magnetite were converted to equivalent surface charge curves and modeled using a simple one-p$K$ model, along with an EDL configuration consisting of a Stern plane containing cations and anions which can specifically bind with charged surface groups, and a diffuse layer capacitance predicted from Gouy–Chapman theory. The same model was shown to adequately fit the experimental results reported for magnetite in $KNO_3$ media by Blesa et al. (1984). An additional cation binding constant permitted a portion of the cation to experience the full surface potential at temperatures above 100°C, as this was needed in order to fit the steep and asymmetrical nature of the charging curves above the $pH_{ppzc}$. This apparent strong interaction of the magnetite surface with $Na^+$ may represent the true nature of the solid surface, or may alternatively be related to a discrepancy between the BET surface area and the true ''reactive'' surface area of the solid, if ions are able to penetrate a significant ''hydrated'' layer on the mineral surface.

The surface charge curves were corrected for an offset presumably due to protolytic impurities in the solid, as was suggested for similar offsets observed in our initial studies of rutile (Machesky et al.,

1994). A second batch of magnetite, exhibiting a significantly higher surface area, did not require this offset correction, and gave background-corrected proton sorption isotherms in 0.03 molal NaTr at 150–250°C that were reversible and nearly coincident with the isotherms obtained with the lower surface area magnetite.

The surface protonation reaction associated with the one-p$K$ model exhibits a negative enthalpy and a large positive heat capacity of reaction ($128 \pm 16$ J $K^{-1}$ $mol^{-1}$), as does rutile (80 J $K^{-1}$ $mol^{-1}$). The result is that the $pH_{ppzc}$ of both solids becomes relatively independent of temperature in the 200–300°C range. As in the case of rutile, the $pH_{ppzc}$ of magnetite roughly parallels $1/2$ p$K_W$ as a function of temperature. These are the only two minerals for which direct potentiometric titration measurements of the proton-induced surface charge are available at temperatures above 95°C. Jayaweera et al. (1994) reported the results of a pioneering study of the streaming potentials in packed powder columns containing a number of minerals at 235°C, from which zeta potentials and points of zero charge were estimated. For magnetite, these authors report a $pH_{pzc}$ of 6.1, somewhat higher than the value of $5.5 \pm 0.3$ estimated in this study. However, for rutile, they report a value of 6.6, compared with the value $4.2 \pm 0.2$ reported by Machesky et al. (1998). Therefore, additional studies at elevated temperatures are needed in order to resolve such discrepancies.

One of the most significant results of this study and our previous studies with rutile (Machesky et al., 1998), is that for a given pH above the point of zero charge, the surface charge density increases significantly with increasing temperature. This can be reasonably related to a combination of closer approach and stronger binding of solution cations to the negatively charged surface with increasing temperature. Furthermore, Ridley et al. (1999) have shown from both surface protonation and direct sampling studies as a function of pH to 250°C, that trace levels of $Ca^{2+}$ in NaCl media at constant ionic strength exhibit a similar strong increase in adsorption for a given pH above the point of zero charge with increasing temperature. These studies suggest that at elevated temperatures, the charging of the mineral surface will play a much more significant role in transport/deposition of colloidal materials and sorption/desorption of ions than at 25°C, where the bulk of all experimental and theoretical investigations have been focused.

Clearly, minerals that are soluble, at least over some pH–temperature range, and redox reactive, pose substantial problems for studies of their surface charging and sorbtive characteristics as a function of temperature, relative to solids such as rutile, which are nearly insoluble and redox insensitive. For such studies, synthesis of a mineral powder with a high surface area is desirable in order to minimize solution blank corrections and other experimental artifacts, but this may also enhance the tendency of the solid to undergo side reactions which consume or produce protons, or otherwise affect the mineral surface, independently of reversible proton sorption at the surface. Within these constraints, this study demonstrates that it is possible to obtain useful information on the surface charge of relatively reactive metal oxides at temperatures to 290°C, which are consistent with other published results over significant temperature ranges.

## Acknowledgements

This study was funded in part by the Office of Basic Energy Sciences, US Department of Energy, under contract DE-AC05-96OR22464 with Oak Ridge National Laboratory, managed by Lockheed Martin Energy Research. MLM also received support from the Illinois State Water Survey and the Illinois Department of Natural Resources, as well as the National Science Foundation (EAR-9627784). The authors wish to thank Dr. J. Stucki of the University of Illinois and B. Moskowitz of the University of Minnesota for their help in characterizing the solid phases used in this study, and also Dr. J.P. Jolivet of the Université Pierre and Marie Curie for providing an unpublished manuscript on the magnetite structure and surface protonation constants. We also thank Dr. T. Hiemstra and W.H. Van Riemsdijk of Wageningen Agricultural University for many helpful discussions. This manuscript was greatly improved by thorough reviews by Jean Pierre Jolivet and Dimitri Sverjensky.

## Appendix A. Experimental results from magnetite proton sorption titrations

| Run# | $T$ (°C) | Ionic strength[a] | μmol $H^+/m^{2b}$ | Error[c] | μmol $H^+/m^{2d}$ | pH[e] |
|---|---|---|---|---|---|---|
| 27 | 149.73 | 0.0300 | 10.825 | 0.705 | 7.999 | 8.385 |
| | 149.73 | 0.0299 | 9.743 | 0.544 | 7.090 | 8.118 |
| | 149.73 | 0.0298 | 8.786 | 0.455 | 6.360 | 7.883 |
| | 149.73 | 0.0298 | 7.882 | 0.396 | 5.721 | 7.650 |
| | 149.73 | 0.0298 | 7.112 | 0.358 | 5.221 | 7.429 |
| | 149.75 | 0.0297 | 6.473 | 0.338 | 4.921 | 7.158 |
| | 149.74 | 0.0297 | 5.918 | 0.320 | 4.619 | 6.950 |
| | 149.74 | 0.0297 | 5.284 | 0.301 | 4.290 | 6.685 |
| | 149.74 | 0.0297 | 4.754 | 0.288 | 4.052 | 6.402 |
| | 149.74 | 0.0297 | 4.348 | 0.273 | 3.793 | 6.245 |
| | 149.74 | 0.0297 | 3.869 | 0.261 | 3.574 | 5.923 |
| | 149.74 | 0.0297 | 3.501 | 0.249 | 3.369 | 5.677 |
| | 149.74 | 0.0297 | 3.042 | 0.233 | 3.079 | 5.356 |
| | 149.74 | 0.0297 | 2.586 | 0.213 | 2.733 | 5.090 |
| | 149.74 | 0.0297 | 1.784 | 0.172 | 2.011 | 4.859 |
| | 149.74 | 0.0297 | 0.031 | 0.076 | 0.333 | 4.634 |
| | 149.74 | 0.0298 | −2.291 | 0.173 | −1.938 | 4.489 |
| | 149.74 | 0.0298 | −6.110 | 0.399 | −5.706 | 4.357 |
| 28 | 149.74 | 0.0300 | 10.491 | 0.672 | 7.902 | 8.372 |
| | 149.74 | 0.0299 | 9.419 | 0.524 | 6.998 | 8.101 |
| | 149.75 | 0.0298 | 8.493 | 0.442 | 6.275 | 7.874 |
| | 149.75 | 0.0298 | 7.571 | 0.383 | 5.604 | 7.634 |
| | 149.74 | 0.0297 | 6.848 | 0.348 | 5.119 | 7.422 |
| | 149.75 | 0.0297 | 6.049 | 0.315 | 4.596 | 7.180 |
| | 149.75 | 0.0297 | 5.317 | 0.289 | 4.163 | 6.912 |
| | 149.74 | 0.0297 | 4.554 | 0.263 | 3.702 | 6.621 |
| | 149.74 | 0.0297 | 3.904 | 0.242 | 3.334 | 6.315 |
| | 149.75 | 0.0297 | 3.403 | 0.226 | 3.049 | 6.042 |
| | 149.75 | 0.0297 | 2.816 | 0.207 | 2.716 | 5.636 |
| | 149.75 | 0.0297 | 2.422 | 0.193 | 2.465 | 5.335 |
| | 149.74 | 0.0297 | 1.717 | 0.160 | 1.887 | 4.982 |
| | 149.74 | 0.0297 | 0.776 | 0.110 | 1.014 | 4.767 |
| | 149.74 | 0.0297 | −0.210 | 0.056 | 0.063 | 4.648 |
| | 149.74 | 0.0298 | −2.560 | 0.186 | −2.234 | 4.486 |
| 30 | 99.78 | 0.0299 | 8.745 | 0.664 | 6.500 | 9.061 |
| | 99.77 | 0.0298 | 7.748 | 0.477 | 5.599 | 8.787 |
| | 99.77 | 0.0297 | 6.944 | 0.372 | 4.916 | 8.500 |
| | 99.79 | 0.0297 | 6.273 | 0.318 | 4.402 | 8.232 |
| | 99.79 | 0.0297 | 5.698 | 0.287 | 4.015 | 7.988 |
| | 99.78 | 0.0296 | 5.143 | 0.267 | 3.700 | 7.729 |
| | 99.78 | 0.0296 | 4.614 | 0.249 | 3.404 | 7.504 |
| | 99.76 | 0.0296 | 4.023 | 0.230 | 3.065 | 7.271 |
| | 99.77 | 0.0296 | 3.487 | 0.214 | 2.778 | 7.039 |
| | 99.78 | 0.0296 | 2.866 | 0.197 | 2.480 | 6.712 |

| | | | | | | |
|---|---|---|---|---|---|---|
| | 99.78 | 0.0296 | 2.123 | 0.176 | 2.114 | 6.223 |
| | 99.78 | 0.0296 | 1.560 | 0.156 | 1.757 | 5.799 |
| | 99.78 | 0.0296 | 1.170 | 0.138 | 1.442 | 5.566 |
| | 99.78 | 0.0296 | 0.443 | 0.100 | 0.771 | 5.332 |
| | 99.77 | 0.0296 | −0.724 | 0.077 | −0.355 | 5.135 |
| | 99.78 | 0.0297 | −2.778 | 0.197 | −2.375 | 4.959 |
| | 99.78 | 0.0297 | −6.067 | 0.392 | −5.633 | 4.810 |
| 31 | 199.86 | 0.0302 | 11.725 | 0.692 | 9.318 | 7.930 |
| | 199.86 | 0.0301 | 10.365 | 0.556 | 7.978 | 7.693 |
| | 199.86 | 0.0301 | 9.288 | 0.471 | 6.984 | 7.487 |
| | 199.86 | 0.0300 | 8.403 | 0.413 | 6.227 | 7.285 |
| | 199.86 | 0.0300 | 7.533 | 0.366 | 5.526 | 7.080 |
| | 199.86 | 0.0300 | 6.763 | 0.331 | 4.957 | 6.878 |
| | 199.86 | 0.0300 | 6.150 | 0.306 | 4.536 | 6.703 |
| | 199.86 | 0.0300 | 5.648 | 0.288 | 4.223 | 6.545 |
| | 199.86 | 0.0300 | 5.170 | 0.271 | 3.934 | 6.393 |
| | 199.86 | 0.0300 | 4.514 | 0.251 | 3.580 | 6.163 |
| | 199.86 | 0.0300 | 3.909 | 0.233 | 3.263 | 5.947 |
| | 199.85 | 0.0300 | 3.217 | 0.214 | 2.930 | 5.681 |
| | 199.85 | 0.0300 | 2.710 | 0.202 | 2.710 | 5.464 |
| | 199.86 | 0.0300 | 2.036 | 0.187 | 2.432 | 5.148 |
| | 199.85 | 0.0300 | 1.513 | 0.170 | 2.141 | 4.947 |
| | 199.85 | 0.0300 | 0.962 | 0.151 | 1.802 | 4.745 |
| | 199.85 | 0.0300 | 0.317 | 0.121 | 1.268 | 4.629 |
| | 199.85 | 0.0300 | −0.598 | 0.076 | 0.482 | 4.484 |
| | 199.86 | 0.0300 | −4.044 | 0.216 | −2.786 | 4.255 |
| 32 | 249.88 | 0.0308 | 14.070 | 0.813 | 11.398 | 7.763 |
| | 249.88 | 0.0307 | 12.370 | 0.654 | 9.568 | 7.550 |
| | 249.89 | 0.0306 | 11.119 | 0.555 | 8.320 | 7.360 |
| | 249.89 | 0.0306 | 10.084 | 0.484 | 7.337 | 7.181 |
| | 249.89 | 0.0305 | 9.068 | 0.423 | 6.413 | 6.972 |
| | 249.89 | 0.0305 | 8.271 | 0.380 | 5.715 | 6.792 |
| | 249.88 | 0.0305 | 7.538 | 0.343 | 5.104 | 6.611 |
| | 249.89 | 0.0305 | 6.712 | 0.305 | 4.449 | 6.414 |
| | 249.89 | 0.0305 | 5.977 | 0.276 | 3.936 | 6.219 |
| | 249.89 | 0.0305 | 5.226 | 0.246 | 3.421 | 6.053 |
| | 249.89 | 0.0305 | 4.358 | 0.222 | 2.985 | 5.807 |
| | 249.89 | 0.0305 | 3.622 | 0.203 | 2.660 | 5.606 |
| | 249.89 | 0.0305 | 2.735 | 0.188 | 2.381 | 5.330 |
| | 249.88 | 0.0305 | 2.080 | 0.177 | 2.172 | 5.123 |
| | 249.88 | 0.0305 | 1.114 | 0.155 | 1.785 | 4.804 |
| | 249.87 | 0.0305 | 0.413 | 0.129 | 1.316 | 4.631 |
| | 249.88 | 0.0305 | −0.502 | 0.087 | 0.578 | 4.454 |
| | 249.88 | 0.0305 | −1.652 | 0.082 | −0.462 | 4.317 |
| | 249.89 | 0.0305 | −3.106 | 0.165 | −1.823 | 4.201 |
| 35 | 290.04 | 0.0315 | 12.653 | 0.809 | 9.235 | 7.952 |
| | 290.05 | 0.0313 | 10.954 | 0.518 | 6.290 | 7.679 |
| | 290.06 | 0.0311 | 9.567 | 0.357 | 4.426 | 7.440 |

| | | | | | | |
|---|---|---|---|---|---|---|
| | 290.05 | 0.0310 | 8.169 | 0.242 | 2.945 | 7.111 |
| | 290.05 | 0.0310 | 7.195 | 0.196 | 2.271 | 6.827 |
| | 290.07 | 0.0310 | 6.311 | 0.175 | 1.924 | 6.539 |
| | 290.05 | 0.0310 | 5.486 | 0.162 | 1.696 | 6.284 |
| | 290.05 | 0.0310 | 4.364 | 0.152 | 1.491 | 5.934 |
| | 290.05 | 0.0309 | 3.226 | 0.145 | 1.359 | 5.556 |
| | 290.05 | 0.0309 | 2.463 | 0.135 | 1.171 | 5.324 |
| | 290.05 | 0.0309 | 1.765 | 0.125 | 0.981 | 5.089 |
| | 290.04 | 0.0309 | 0.779 | 0.095 | 0.450 | 4.832 |
| | 290.05 | 0.0309 | −0.347 | 0.089 | −0.311 | 4.569 |
| | 290.05 | 0.0309 | −2.392 | 0.201 | −2.175 | 4.409 |
| | 290.05 | 0.0309 | −4.414 | 0.314 | −4.025 | 4.174 |
| 36 | 49.77 | 0.0299 | 9.490 | 0.600 | 4.493 | 10.063 |
| | 49.78 | 0.0299 | 9.468 | 0.539 | 4.513 | 9.983 |
| | 49.78 | 0.0297 | 9.218 | 0.413 | 4.419 | 9.743 |
| | 49.78 | 0.0297 | 7.805 | 0.268 | 3.242 | 9.394 |
| | 49.78 | 0.0296 | 6.309 | 0.179 | 2.211 | 8.642 |
| | 49.79 | 0.0296 | 5.844 | 0.164 | 1.960 | 8.289 |
| | 49.79 | 0.0296 | 5.338 | 0.152 | 1.748 | 7.878 |
| | 49.79 | 0.0296 | 4.731 | 0.138 | 1.491 | 7.485 |
| | 49.78 | 0.0296 | 3.989 | 0.121 | 1.189 | 7.071 |
| | 49.79 | 0.0296 | 3.240 | 0.094 | 0.714 | 6.835 |
| | 49.77 | 0.0296 | 2.226 | 0.062 | 0.146 | 6.459 |
| | 49.80 | 0.0296 | 1.136 | 0.081 | −0.460 | 6.015 |
| | 49.79 | 0.0296 | 0.467 | 0.115 | −1.024 | 5.903 |
| | 49.79 | 0.0296 | −0.593 | 0.165 | −1.864 | 5.628 |
| | 49.79 | 0.0296 | −2.355 | 0.261 | −3.459 | 5.332 |
| 37 | 49.74 | 0.0299 | 8.277 | 0.549 | 3.307 | 10.087 |
| | 49.86 | 0.0299 | 8.253 | 0.510 | 3.306 | 10.039 |
| | 49.88 | 0.0298 | 7.916 | 0.364 | 3.103 | 9.813 |
| | 49.88 | 0.0297 | 7.194 | 0.245 | 2.604 | 9.490 |
| | 49.87 | 0.0296 | 6.599 | 0.190 | 2.207 | 9.196 |
| | 49.86 | 0.0296 | 6.054 | 0.160 | 1.851 | 8.887 |
| | 49.81 | 0.0296 | 5.500 | 0.137 | 1.500 | 8.538 |
| | 49.81 | 0.0296 | 4.923 | 0.122 | 1.237 | 8.050 |
| | 49.84 | 0.0296 | 4.063 | 0.101 | 0.870 | 7.468 |
| | 49.86 | 0.0296 | 3.416 | 0.084 | 0.553 | 7.150 |
| | 49.84 | 0.0296 | 2.751 | 0.062 | 0.167 | 6.904 |
| | 49.84 | 0.0296 | 1.416 | 0.086 | −0.563 | 6.388 |
| | 49.64 | 0.0296 | 0.079 | 0.146 | −1.554 | 6.065 |
| | 49.64 | 0.0296 | −1.917 | 0.248 | −3.259 | 5.735 |
| | 49.63 | 0.0296 | −4.566 | 0.396 | −5.731 | 5.459 |
| | 49.62 | 0.0296 | −11.214 | 0.786 | −12.267 | 5.165 |
| 38 | 99.79 | 0.0299 | 8.649 | 0.656 | 6.433 | 9.060 |
| | 99.79 | 0.0298 | 7.777 | 0.472 | 5.665 | 8.766 |
| | 99.79 | 0.0297 | 7.005 | 0.374 | 5.015 | 8.478 |
| | 99.79 | 0.0297 | 6.379 | 0.324 | 4.563 | 8.189 |
| | 99.79 | 0.0296 | 5.708 | 0.292 | 4.132 | 7.891 |

| | | | | | | |
|---|---|---|---|---|---|---|
| | 99.79 | 0.0296 | 4.717 | 0.256 | 3.539 | 7.489 |
| | 99.79 | 0.0296 | 4.187 | 0.237 | 3.210 | 7.301 |
| | 99.79 | 0.0296 | 3.413 | 0.211 | 2.743 | 7.010 |
| | 99.78 | 0.0296 | 2.649 | 0.187 | 2.326 | 6.646 |
| | 99.78 | 0.0296 | 1.999 | 0.168 | 1.989 | 6.225 |
| | 99.78 | 0.0296 | 1.410 | 0.147 | 1.622 | 5.752 |
| | 99.78 | 0.0296 | 0.710 | 0.113 | 1.016 | 5.414 |
| | 99.78 | 0.0296 | 0.043 | 0.076 | 0.385 | 5.246 |
| | 99.79 | 0.0296 | −1.813 | 0.139 | −1.424 | 5.003 |
| | 99.80 | 0.0297 | −6.604 | 0.423 | −6.167 | 4.767 |
| 40 | 24.97 | 0.0299 | 9.376 | 0.664 | 4.685 | 10.790 |
| | 24.95 | 0.0298 | 10.025 | 0.579 | 5.493 | 10.630 |
| | 24.95 | 0.0297 | 9.786 | 0.468 | 5.688 | 10.354 |
| | 25.00 | 0.0297 | 8.519 | 0.371 | 4.778 | 10.153 |
| | 25.00 | 0.0296 | 7.378 | 0.307 | 4.271 | 9.764 |
| | 25.00 | 0.0296 | 5.673 | 0.238 | 3.191 | 8.985 |
| | 25.01 | 0.0296 | 4.601 | 0.188 | 2.322 | 8.001 |
| | 25.01 | 0.0296 | 3.930 | 0.169 | 1.988 | 7.478 |
| | 25.01 | 0.0296 | 3.239 | 0.149 | 1.637 | 7.160 |
| | 25.01 | 0.0296 | 1.852 | 0.109 | 0.925 | 6.664 |
| | 25.05 | 0.0296 | 0.455 | 0.066 | −0.166 | 6.452 |
| | 25.05 | 0.0296 | −2.283 | 0.184 | −2.124 | 5.803 |
| 47 | 25.03 | 0.3000 | 4.039 | 0.880 | 5.387 | 11.125 |
| | 25.02 | 0.2994 | 6.407 | 0.718 | 6.315 | 10.902 |
| | 25.01 | 0.2988 | 7.890 | 0.507 | 6.143 | 10.441 |
| | 25.07 | 0.2986 | 7.947 | 0.437 | 5.728 | 9.955 |
| | 25.07 | 0.2985 | 6.766 | 0.375 | 4.747 | 9.329 |
| | 25.05 | 0.2984 | 5.707 | 0.347 | 4.244 | 8.468 |
| | 25.05 | 0.2984 | 3.750 | 0.293 | 3.278 | 6.953 |
| | 25.05 | 0.2984 | 1.108 | 0.184 | 1.371 | 6.022 |
| | 25.06 | 0.2983 | −2.228 | 0.221 | −1.950 | 6.004 |
| | 25.04 | 0.2983 | −5.992 | 0.423 | −5.321 | 5.280 |
| 48 | 149.82 | 0.3011 | 14.047 | 1.081 | 12.205 | 8.605 |
| | 149.82 | 0.3004 | 13.387 | 0.809 | 10.255 | 8.333 |
| | 149.81 | 0.3001 | 12.503 | 0.635 | 8.648 | 8.060 |
| | 149.82 | 0.2999 | 11.596 | 0.545 | 7.646 | 7.808 |
| | 149.81 | 0.2998 | 10.550 | 0.489 | 6.894 | 7.524 |
| | 149.81 | 0.2997 | 9.717 | 0.458 | 6.404 | 7.299 |
| | 149.81 | 0.2997 | 8.784 | 0.426 | 5.856 | 7.038 |
| | 149.82 | 0.2997 | 7.728 | 0.387 | 5.169 | 6.729 |
| | 149.82 | 0.2996 | 6.592 | 0.341 | 4.370 | 6.371 |
| | 149.81 | 0.2996 | 5.246 | 0.289 | 3.443 | 5.892 |
| | 149.81 | 0.2996 | 3.924 | 0.238 | 2.554 | 5.395 |
| | 149.81 | 0.2996 | 2.574 | 0.179 | 1.519 | 4.982 |
| | 149.82 | 0.2995 | 1.207 | 0.109 | 0.288 | 4.794 |
| | 149.82 | 0.2995 | −2.358 | 0.278 | −3.112 | 4.576 |
| | 149.82 | 0.2994 | −8.398 | 0.631 | −9.009 | 4.403 |

| | | | | | | |
|---|---|---|---|---|---|---|
| 49 | 199.94 | 0.3037 | 18.812 | 1.194 | 14.389 | 8.163 |
| | 199.93 | 0.3030 | 17.649 | 0.918 | 12.146 | 7.903 |
| | 199.93 | 0.3025 | 15.958 | 0.731 | 10.372 | 7.590 |
| | 199.92 | 0.3023 | 14.636 | 0.645 | 9.359 | 7.328 |
| | 199.93 | 0.3022 | 13.359 | 0.588 | 8.538 | 7.005 |
| | 199.93 | 0.3021 | 12.001 | 0.534 | 7.628 | 6.667 |
| | 199.93 | 0.3020 | 9.897 | 0.457 | 6.278 | 6.128 |
| | 199.92 | 0.3020 | 8.625 | 0.410 | 5.455 | 5.855 |
| | 199.92 | 0.3020 | 7.295 | 0.362 | 4.613 | 5.582 |
| | 199.92 | 0.3019 | 5.898 | 0.315 | 3.793 | 5.270 |
| | 199.91 | 0.3019 | 4.716 | 0.272 | 3.022 | 5.045 |
| | 199.92 | 0.3019 | 3.025 | 0.201 | 1.784 | 4.791 |
| | 199.91 | 0.3018 | 0.240 | 0.138 | −0.645 | 4.592 |
| | 199.92 | 0.3017 | −3.425 | 0.343 | −4.065 | 4.457 |
| | 199.92 | 0.3016 | −8.735 | 0.648 | −9.166 | 4.344 |
| 50 | 249.46 | 0.3104 | 21.005 | 1.300 | 17.704 | 7.918 |
| | 249.46 | 0.3093 | 18.324 | 0.953 | 13.727 | 7.628 |
| | 249.46 | 0.3089 | 16.585 | 0.780 | 11.508 | 7.407 |
| | 249.46 | 0.3086 | 15.364 | 0.678 | 10.084 | 7.208 |
| | 249.46 | 0.3084 | 14.099 | 0.593 | 8.778 | 6.994 |
| | 249.45 | 0.3083 | 13.037 | 0.535 | 7.829 | 6.783 |
| | 249.45 | 0.3082 | 12.295 | 0.500 | 7.236 | 6.644 |
| | 249.45 | 0.3081 | 11.087 | 0.454 | 6.448 | 6.384 |
| | 249.46 | 0.3080 | 9.807 | 0.415 | 5.756 | 6.117 |
| | 249.45 | 0.3080 | 8.539 | 0.381 | 5.156 | 5.862 |
| | 249.46 | 0.3079 | 7.187 | 0.351 | 4.610 | 5.584 |
| | 249.46 | 0.3078 | 5.993 | 0.324 | 4.140 | 5.350 |
| | 249.45 | 0.3078 | 4.583 | 0.296 | 3.632 | 5.069 |
| | 249.46 | 0.3077 | 3.270 | 0.260 | 2.994 | 4.860 |
| | 249.45 | 0.3076 | 1.177 | 0.181 | 1.602 | 4.634 |
| | 249.45 | 0.3074 | −2.253 | 0.166 | −1.256 | 4.425 |
| | 249.46 | 0.3072 | −6.684 | 0.411 | −5.344 | 4.273 |
| 51 | 99.82 | 0.3001 | 11.162 | 0.987 | 9.949 | 9.296 |
| | 99.82 | 0.2996 | 11.267 | 0.787 | 9.092 | 9.075 |
| | 99.81 | 0.2992 | 11.065 | 0.615 | 8.035 | 8.772 |
| | 99.80 | 0.2990 | 10.426 | 0.507 | 6.994 | 8.439 |
| | 99.81 | 0.2989 | 9.729 | 0.455 | 6.296 | 8.122 |
| | 99.81 | 0.2988 | 9.036 | 0.424 | 5.803 | 7.848 |
| | 99.82 | 0.2988 | 8.019 | 0.389 | 5.187 | 7.502 |
| | 99.81 | 0.2987 | 6.801 | 0.347 | 4.444 | 7.142 |
| | 99.81 | 0.2987 | 5.505 | 0.299 | 3.601 | 6.777 |
| | 99.82 | 0.2987 | 4.097 | 0.249 | 2.719 | 6.217 |
| | 99.82 | 0.2987 | 2.675 | 0.184 | 1.585 | 5.692 |
| | 99.83 | 0.2987 | 1.166 | 0.103 | 0.180 | 5.396 |
| | 99.83 | 0.2986 | −0.313 | 0.167 | −1.249 | 5.234 |
| | 99.82 | 0.2986 | −3.063 | 0.328 | −3.938 | 5.036 |
| | 99.84 | 0.2985 | −8.023 | 0.620 | −8.826 | 4.824 |

| | | | | | | |
|---|---|---|---|---|---|---|
| 54 | 289.92 | 0.3168 | 16.792 | 1.112 | 12.390 | 8.024 |
| | 289.92 | 0.3156 | 18.874 | 0.936 | 11.815 | 7.805 |
| | 289.91 | 0.3146 | 17.655 | 0.660 | 8.808 | 7.515 |
| | 289.91 | 0.3140 | 16.465 | 0.515 | 7.032 | 7.232 |
| | 289.91 | 0.3135 | 14.055 | 0.385 | 5.077 | 6.682 |
| | 289.91 | 0.3133 | 12.035 | 0.314 | 3.848 | 6.391 |
| | 289.91 | 0.3131 | 9.810 | 0.266 | 2.990 | 6.055 |
| | 289.92 | 0.3128 | 6.160 | 0.218 | 2.110 | 5.558 |
| | 289.92 | 0.3126 | 3.751 | 0.219 | 2.084 | 5.160 |
| | 289.92 | 0.3125 | 1.485 | 0.168 | 1.152 | 4.882 |
| | 289.92 | 0.3123 | −0.642 | 0.111 | −0.124 | 4.472 |
| 55 | 49.65 | 0.2999 | 8.578 | 0.734 | 5.279 | 10.353 |
| | 49.65 | 0.2993 | 9.939 | 0.609 | 5.906 | 10.130 |
| | 49.56 | 0.2989 | 10.819 | 0.485 | 6.020 | 9.767 |
| | 49.57 | 0.2987 | 10.233 | 0.399 | 5.155 | 9.502 |
| | 49.54 | 0.2986 | 9.454 | 0.336 | 4.287 | 9.211 |
| | 49.55 | 0.2985 | 8.351 | 0.279 | 3.369 | 8.767 |
| | 49.55 | 0.2985 | 7.432 | 0.252 | 2.893 | 8.315 |
| | 49.82 | 0.2985 | 5.974 | 0.230 | 2.485 | 7.516 |
| | 49.81 | 0.2984 | 4.201 | 0.178 | 1.556 | 6.881 |
| | 49.80 | 0.2984 | 2.219 | 0.099 | 0.180 | 6.365 |
| | 49.70 | 0.2984 | 0.248 | 0.177 | −1.484 | 6.062 |
| | 49.67 | 0.2984 | −1.831 | 0.294 | −3.441 | 5.927 |
| | 49.66 | 0.2983 | −6.413 | 0.551 | −7.734 | 5.577 |
| 93 | 149.91 | 0.0293 | 11.617 | 0.723 | 8.938 | 8.330 |
| | 149.90 | 0.0292 | 10.348 | 0.574 | 7.840 | 8.080 |
| | 149.90 | 0.0292 | 9.021 | 0.467 | 6.782 | 7.802 |
| | 149.91 | 0.0291 | 7.587 | 0.387 | 5.741 | 7.457 |
| | 149.91 | 0.0291 | 6.227 | 0.328 | 4.807 | 7.099 |
| | 149.91 | 0.0291 | 5.329 | 0.293 | 4.204 | 6.841 |
| | 149.91 | 0.0291 | 4.628 | 0.267 | 3.751 | 6.608 |
| | 149.91 | 0.0291 | 3.822 | 0.237 | 3.208 | 6.336 |
| | 149.91 | 0.0291 | 3.095 | 0.210 | 2.743 | 6.017 |
| | 149.91 | 0.0291 | 2.402 | 0.183 | 2.267 | 5.690 |
| | 149.91 | 0.0292 | 1.642 | 0.152 | 1.729 | 5.235 |
| | 149.91 | 0.0292 | 0.907 | 0.117 | 1.105 | 4.924 |
| | 149.91 | 0.0292 | 0.160 | 0.077 | 0.412 | 4.754 |
| | 149.91 | 0.0292 | −1.472 | 0.123 | −1.160 | 4.567 |
| | 149.91 | 0.0292 | −3.472 | 0.241 | −3.114 | 4.435 |
| | 149.91 | 0.0292 | −5.340 | 0.351 | −4.952 | 4.358 |

[a] Stoichiometric molal ionic strength.

[b] Micromoles of excess $H^+$ in solution per square meter of magnetite surface, uncorrected.

[c] Uncertainty in calculated excess $H^+$ in solution per square meter of magnetite surface.

[d] Micromoles of excess $H^+$ in solution per square meter of magnetite surface, corrected for background (solution blank) effects.

[e] Measured pH, on the activity scale.

## References


Archer, D.G., 1992. Thermodynamic properties of the $NaCl + H_2O$ system. II. Thermodynamic properties of NaCl(aq), NaCl–$2H_2O$(cr), and phase equilibria. J. Phys. Chem. 21, 793–829.

Baes, C.F. Jr., Mesmer, R.E., 1986. The Hydrolysis of Cations. Krieger, Malabar, FL, Reprint edn. 489 pp.

Berube, Y.G., de Bruyn, P.L., 1968. Adsorption at the rutile–solution interface: I. Thermodynamic and experimental study. J. Colloid Interface Sci. 27, 305–318.

Blesa, M.A., Néstor, M.F., Maroto, A.J.G., Regazzoni, A.E., 1984. The influence of temperature on the interface magnetite–aqueous electrolyte solution. J. Colloid Interface Sci. 101, 410–418.

Bolt, G.H., Van Riemsdijk, W.H., 1982. Ion adsorption on inorganic variable charge minerals. In: Bolt, G.H. (Ed.), Soil Chemistry Part B: Physico-Chemical Models. Elsevier, Amsterdam, pp. 459–504.

Busey, R.H., Mesmer, R.E., 1978. Thermodynamic quantities for the ionization of water in sodium chloride media to 300°C. J. Chem. Eng. Data 23, 175–176.

Catalette, H., Dumonceau, J., Ollar, P., 1998. Sorption of cesium, barium and europium on magnetite. J. Contam. Hydrol. 35, 151–159.

Cornell, R.M., Schwertmann, U., 1996. The Iron Oxides. VCH Publishers, New York, 573 pp.

Dresco, P.A., Zaitsev, V.S., Gambino, R.J., Chu, B., 1999. Preparation and properties of magnetite and polymer magnetite nanoparticles. Langmuir 15, 1945–1951.

Dzombak, D.A., Morel, F.M.M., 1990. Surface Complexation Modeling: Ferric Oxide. New York, Wiley, 393 pp.

Ely, J.F., Huber, M.L., 1990. NIST Thermophysical Properties of Hydrocarbon Mixtures Database (SUPERTRAPP), NIST Standard Reference Database 4, User's Guide, Version 1.0. US Department of Commerce, National Institute of Standards and Technology, 44 pp.

Fabes, L., Swaddle, T.W., 1975. Reagents for high temperature aqueous chemistry: trifluoromethanesulfonic acid and its salts. Can. J. Chem. 53, 3053–3059.

Fokkink, L.G.J, 1987. Ion adsorption on oxides: Surface charge formation and cadmium binding on rutile and hematite. PhD thesis, Wageningen Agricultural University, Wageningen, The Netherlands.

Fokkink, L.G.J., de Keizer, A., Lyklema, J., 1989. Temperature dependence of the electrical double layer on oxides: rutile and hematite. J. Colloid Interface Sci. 127, 116–131.

Heinrich, C.A., Seward, T.M., 1990. A spectrophotometric study of aqueous iron(II) chloride complexing from 25 to 200°C. Geochim. Cosmochim. Acta 54, 2207–2221.

Hiemstra, T., Van Riemsdijk, W.H., Bolt, H.G., 1989. Multisite proton adsorption modeling at the solid/solution interface of (hydr)oxides: I. Model description and intrinsic reaction constants. J. Colloid Interface Sci. 133, 91–104.

Hiemstra, T., Venema, P., Van Riemansdijk, W.H., 1996. Intrinsic proton affinity of reactive surface groups of metal (hydr)oxides: the bond valence principle. J. Colloid Interface Sci. 184, 680–692.

Hiemstra, T., Yong, T., Van Riemsdijk, W.H., 1999. The interfacial charging phenomena of Al (hydr)oxides. Langmuir, (in press).

Ho, P.C., Palmer, D.A., 1995. Electrical conductivity measurements of dilute aqueous trifluoromethanesulfonate solutions at temperatures 0–450°C and pressures up to 250 MPa. J. Solution Chem. 24, 753–769.

Huebner, J.S., 1971. Buffering techniques for hydrostatic systems at elevated temperatures. In: Ulmer, G.C. (Ed.), Research Techniques for High Pressure and Temperature. Springer-Verlag, New York, pp. 123–177.

Jayaweera, P., Hettiarachchi, S., Ocken, H., 1994. Determination of the high temperature zeta potential and pH of zero charge of some transition metal oxides. Colloids Surf. A 85, 19–27.

Jolivet, J.P., Hernandez, J., 1999. Modeling of surface acid–base properties of magnetite in aqueous medium. Unpublished manuscript.

Jolivet, J.-P., Tronc, E., 1988. Interfacial electron transfer in colloidal spinel iron oxide. Conversion of $Fe_3O_{4-\gamma}Fe_2O_3$ in aqueous medium. J. Colloid Interface Sci. 125, 688–701.

Lyklema, J., 1961. Geometrical factors in the capacity of the electrical double layer. Kolloid-Z. 175, 129.

Lyklema, J., 1984. Points of zero charge in the presence of specific adsorption. J. Colloid Interface Sci. 99, 109–117.

Machesky, M.L., Palmer, D.A., Wesolowski, D.J., 1994. Hydrogen ion adsorption at the rutile–water interface to 250°C. Geochim. Cosmochim. Acta 58, 5627.

Machesky, M.L., Wesolowski, D.J., Palmer, D.A., 1998. Potentiometric titrations of rutile suspensions to 250°C. J. Colloid Interface Sci. 200, 298–309.

Machesky, M.L., Wesolowski, D.J., Palmer, D.A., 2000. On the temperature dependence of intrinsic surface protonation equilibrium constants: an extension of the refined MUSIC model. Manuscript in preparation.

Mackor, E.I., 1951. The properties of the electrical double layer: III. The capacity of the double layer on Hg and AgI. Recl. Trav. Chim. 70, 763.

Marmier, N., Delisée, A., Fromage, F., 1999. Surface complexation modeling of Yb(III), Ni(II) and Cs(I) sorption on magnetite. J. Colloid Interface Sci. 211, 54–60.

Mathur, B.S., Venkataramani, B., 1998. Surface charge and surface chemical characteristics of magnetites substituted with nickel, cobalt and chromium. Colloids Surf. A 140, 403–416.

Mesmer, R.E., Holmes, H.F., 1992. pH, definition and measurement at high temperatures. J. Solution Chem. 21, 725–744.

Mesmer, R.E., Baes, C.F. Jr., Sweeton, F.H., 1970. Acidity measurements at elevated temperatures: IV. Apparent dissociation constants of water in 1 m potassium chloride up to 292°C. J. Phys. Chem. 74, 937.

Mesmer, R.E., Palmer, D.A., Wesolowski, D.J., 1995. Potentiometric studies at ORNL with hydrogen-electrode concentration cells. In: White, H.J., Sengers, J.V., Neumann, D.B., Bellows, J.C. (Eds.), Proc. 12th Intern. Conf. Properties Water and Steam. Begell House, New York, pp. 423–431.

Onoda, G.Y., deBruyn, P.L., 1966. Proton adsorption at the ferric oxide/aqueous solution interface: I. A kinetic study of adsorption. Surf. Sci. 4, 48–63.

Palmer, D.A., Bénézeth, P., Wesolowski, D.J., 2000. Aqueous high temperature solubility studies. I. The solubility of

boehmite as functions of ionic strength (to 5 molal, NaCl), temperature (100–250°C), and pH as determined by in situ measurements. Manuscript in preparation.

Palmer, D.A., Drummond, S.E., 1988. The molal dissociation quotients of water in sodium trifluoromethanesulfonate solutions to high temperatures. J. Solution Chem. 17, 153–164.

Palmer, D.A., Hyde, K.E., 1993. Ferrous chloride and acetate complexation in aqueous solutions at high temperatures. Geochim. Cosmochim. Acta 57, 1393–1408.

Parks, G.A., 1965. The isoelectric points of solid oxides, solid hydroxides, and aqueous hydroxo complex systems. Chem. Rev. 65, 177–198.

Parks, G.A., de Bruyn, P.L., 1962. The zero point of charge of oxides. J. Phys. Chem. 66, 967–973.

Quist, A.S., Marshall, W.L., 1965. Assignment of limiting equivalent conductances for single ions to 400°C. J. Phys. Chem. 69, 2984–2987.

Regazzoni, A.E., Blesa, M.A., Maroto, A.J.G., 1983. Interfacial properties of zirconium dioxide and magnetite in water. J. Colloid Interface Sci. 91, 560–570.

Regazzoni, A.E., Urrutia, G.A., Blesa, M.A., Maroto, A.J.G., 1981. Some observations on the composition and morphology of synthetic magnetites obtained by different routes. J. Inorg. Nucl. Chem. 43, 1489.

Ridley, M.K., Machesky, M.L., Wesolowski, D.J., Palmer, D.A., 1999. Ca(II) adsorption at the rutile–water interface: a potentiometric study in NaCl media to 250°C. Geochim. Cosmochim. Acta 63, 3087–3096.

Schoonen, M.A.A., 1994. Calculation of the point of zero charge of metal oxides between 0 and 350°C. Geochim. Cosmochim. Acta 58, 2845–2851.

Shen, J., Ebner, A.D., Ritter, J.A., 1999. Points of zero charge and intrinsic equilibrium constants of silica–magnetite composite oxides. J. Colloid Interface Sci. 214, 333–343.

Shock, E.L., Sassani, D.C., Willis, M., Sverjensky, D.A., 1997. Inorganic species in geologic fluids: correlations among standard molal thermodynamic properties of aqueous ions and hydroxide complexes. Geochim. Cosmochim. Acta 61, 907–950.

Sposito, G., 1998. On points of zero charge. Environ. Sci. Technol. 32, 2815–2819.

Stumm, W., 1992. Chemistry of the Solid–Water Interface: Processes at the Mineral–Water and Particle–Water Interface in Natural Systems. Wiley, New York, 428 pp.

Sverjensky, D.A., Sahai, N., 1996. Theoretical prediction of single-site surface-protonation equilibrium constants for oxides and silicates in water. Geochim. Cosmochim. Acta 60, 3773–3797.

Sverjensky, D.A., Sahai, N., 1998. Theoretical prediction of single-site enthalpies of surface protonation for oxides and silicates in water. Geochim. Cosmochim. Acta 62, 3703–3716.

Swaddle, T.W., Oltmann, P., 1980. Kinetics of magnetite–maghemite–hematite transformation, with special reference to hydrothermal systems. Can. J. Chem. 58, 1763–1772.

Tamaura, Y., Tabata, M., 1990. Complete reduction of carbon dioxide to carbon using cation-excess magnetite. Nature 346, 255–256.

Tewari, P.H., McLean, A.W., 1972. Temperature dependence of point of zero charge of alumina and magnetite. J. Colloid Interface Sci. 40, 267–272.

Tremaine, P.R., LeBlanc, J.C., 1980. The solubility of magnetite and the hydrolysis and oxidation of $Fe^{2+}$ in water to 300°C. J. Solution Chem. 9, 415–442.

Vayssières, L., Chanéac, C., Tronc, E., Jolivet, J.P., 1998. Size tailoring of magnetite particles formed by aqueous precipitation: an example of thermodynamic stability of nanometric oxide particles. J. Colloid Interface Sci. 205, 205–212.

Wesolowski, D.J., Bénézeth, P., Palmer, D.A., 1998. ZnO solubility and $Zn^{2+}$ complexation by chloride and sulfate in acidic solutions to 290°C with in situ pH measurement. Geochim. Cosmochim. Acta 62, 971–984.

Wesolowski, D.J., Palmer, D.A., Mesmer, R.E., 1995. Measurement and control of pH in hydrothermal solutions. In: Proc. 8th Intern. Symp. Water–Rock Interaction, Vladivostok, Russia. A.A. Balkema, pp. 51–55, Keynote Address.

White, A.F., Peterson, M.L., Hochella, M.F., 1994. Electrochemistry and dissolution kinetics of magnetite and ilmenite. Geochim. Cosmochim. Acta 58, 1859–1876.

Ziemniak, S.E., Jones, M.E., Combs, K.E.S., 1995. Magnetite solubility and phase stability in alkaline media at elevated temperatures. J. Solution Chem. 24, 837–877.